ROYAL SOCIETY OF CHEMISTRY

PAPER

Check for updates

Insight into the synergetic, steric and energetic properties of zeolitization and cellulose fiber functionalization of diatomite during the adsorption of Cd(II): advanced equilibrium studies†

Mostafa R. Abukhadra, [ID] *[ab] Islam Saad,[bc] Sarah I. Al Othman,[d] Haifa E. Alfassam[d] and Ahmed A. Allam[e]

The adsorption potentiality of zeolitized diatomite (ZD) frustules and their cellulose hybridized (C/ZD) product for Cd(II) ions was assessed in synergetic studies to investigate the impact of the modification processes. The adsorption properties were illustrated based on the steric and energetic parameters of the applied advanced equilibrium modeling (monolayer model of one energy). The cellulose hybridization process increased the adsorption properties of Cd(II) significantly to 229.4 mg g^{-1} as compared to ZD (180.8 mg g^{-1}) and raw diatomite (DA) (127.8 mg g^{-1}) during the saturation state. The steric investigation suggested a notable increase in the quantities of the active sites after the zeolitization (N_m = 62.37 mg g^{-1}) and cellulose functionalization (N_m = 98.46 mg g^{-1}), which illustrates enhancement in the Cd(II) uptake capacity of C/ZD. Moreover, each active site of C/ZD can absorb about 4 ions of Cd(II) ZD, which occur in a vertical orientation. The energetic studies, including Gaussian energy (<8 kJ mol^{-1}) and retention energy (<8 kJ mol^{-1}), demonstrate the physical uptake of Cd(II), which might involve cooperating van der Waals forces (4–10 kJ mol^{-1}), hydrophobic bonds (5 kJ mol^{-1}), dipole forces (2–29 kJ mol^{-1}), and hydrogen bonding (<30 kJ mol^{-1}) in addition to zeolitic ion exchange mechanisms (0.6–25 kJ mol^{-1}). The behaviors and values of entropy, internal energy, and free enthalpy as the assessed thermodynamic functions validate the exothermic and spontaneous properties of the Cd(II) retention by ZD and the C/ZD composite.

1 Introduction

The extensive contamination of freshwater resources, in addition to its associated hazardous health and environmental impacts, is a critical concern that threatens the safety of the modern world.[1,2] Uncontrolled, extensive, and continuous discharging of polluted effluents that are related to mining, agricultural, and industrial activities represent the main sources and reasons for the water pollution problem and its related environmental phenomena.[3,4] Such discharged effluents are highly saturated with several species of dissolved organic chemical compounds, whether organic (pharmaceutical

residuals, petrochemicals, pesticides, and dyes) or inorganic (heavy metals, phosphate, ammonium, sulfate, and nitrate), and most of them, at their abnormal concentrations, display notable adverse environmental and health impacts.[5,6] The extensive existence of heavy metals as dissolved ions or chemical complexes with other chemicals in water resources represents one of the critical hazardous challenges that threaten the safety of our ecosystem and the health of humanity.[1,7] They were categorized as biodegradable, resistant, highly toxic, and carcinogenic contaminants that tend to accumulate significantly within the tissues of animals and the human body.[7–9] The existence of dissolved metals at a concentration higher than 50 µg L^{-1} displays a carcinogenic impact on the lungs, liver, and kidneys when drinking one liter per day.[10,11] Additionally, they exhibit a destructive impact on the central nervous system as well as the blood cells and skin.[10,12] The pollution of water resources with Cd(II) has been detected widely and is caused essentially by the discharged effluents from numerous industries (smelting, cadmium–nickel batteries, metal plating, pigments, and alloys).[13,14] The Cd(II) was classified as a carcinogenic and very toxic chemical ion that must be at a concentration lower than about 0.003 mg L^{-1} in the drinking water.[4,15]

aGeology Department, Faculty of Science, Beni-Suef University, Beni Suef, Egypt. E-mail: Abukhadra89@Science.bsu.edu.eg

bMaterials Technologies and Their Applications Lab, Faculty of Science, Beni-Suef University, Beni Suef, Egypt

cPhysics Department, Faculty of Science, Beni-Suef University, Beni-Suef, 65211, Egypt

dPrincess Nourah bint Abdulrahman University, College of Science, Biology Department, Riyadh, Saudi Arabia

eZoology Department, Faculty of Science, Beni-Suef University, Beni-Suef, Egypt

Moreover, the Cd(II) pollutants cause several health side effects, such as acute disorders, pulmonary edema, chronic disorders, emphysema, itai-itai disease, hepatic dysfunction, hypertension, testicular atrophy, osteomalacia, and renal damage.[13,16] Environmentally, the Cd(II) ions exhibit remarkable inhibition effects on the germination of seeds, root elongation of plants, plant length, and leaf productivity.[17] Moreover, the unacceptable concentrations of Cd(II) cause strong adverse effects on aquatic life and ecosystems, as well as the economic quality of fish.[14]

Therefore, the effective elimination of the Cd(II) concentration in the water supplies is a critical concern considering the previous reported environmental and health hazards. The adsorption decontamination of dissolved metal ions such as Cd(II) by natural and synthetic adsorbents was recommended in numerous studies as a simple, effective, simple, and low-cost purification technique.[18,19] However, the development of suitable adsorbent materials is still an attractive research point considering the essential qualification criteria such as availability of material, production cost, recyclability, adsorption capacity, kinetic rates, and equilibrium behaviors.[7,20,21] The adsorption of metals using natural raw materials and their modified forms and composites represents the most effective decontamination technique according to availability, cost, escalation, and environmental considerations.[6,22]

Natural and synthetic nano-porous silicate and silica-based materials were extensively inspected as promising adsorbent structures that are characterized by significant surface area, adsorption capacity, and highly porous properties.[23,24] Diatomite is a commonly used geological term to identify the natural accumulation of the siliceous skeletons of the diatom frustules.[25,26] As a material, it is classified as a non-toxic biomaterial and is characterized by notably high natural reserves, surface area, thermo-chemical stability, surface reactivity, and adsorption capacity.[25,27,28] Therefore, it was extensively applied in the significant remediation and retention processes of different species of dissolved chemical ions in the water supplies.[25,29] However, the recently developed studies demonstrate notable enhancement impacts of the phase and surficial modification processes on the textural as well as physicochemical properties of diatomite.[24,30]

The zeolitization transformation of siliceous diatomite frustules completely into synthetic zeolite phases or hybridized forms of zeolite/diatomite has been reported as a promising modification technique that strongly enhances the textural properties (surface area and porosity) as well as the physicochemical properties (adsorption, surface reactivity, and ion exchange capacity).[31–33] Moreover, the polymeric hybridization of such structures with the chains of the biopolymers (chitosan, cellulose, and β-cyclodextrin) commonly produces advanced structures that are characterized by significantly enhanced adsorption capacity, biodegradability, and enrichment in the active sites.[34–37]

Cellulose, cellulose-based materials, and cellulose-functionalized materials were studied recently as promising eco-friendly materials in different medical and environmental applications.[34] It is one of the extensively abundant biopolymers that can be obtained as an extract product by simple and low-cost techniques from numerous green sources such as green plants, biomasses, trees, and agricultural wastes.[38,39] Chemically, it exhibits a polysaccharide polymeric structure in which the bonding between the functional anhydroglucose rings occurs by b-1, 4 glycoside bonds.[40,41] Therefore, cellulose possesses high stability, reactivity, heat resistance, chemical flexibility, and biodegradability.[42,43] The high reactivity and chemical flexibility of the cellulose structure qualify it to be effectively integrated into different hybridized structures, either of an inorganic or organic nature.[38]

Therefore, the introduced study involved a deep investigation for the characterization of three diatomite bases as adsorbents for Cd(II) in the aqueous environment. The three adsorbents were produced by phase modification of diatomite and functionalization of the modified structure with cellulose (raw diatomite (DA), zeolitized diatomite (ZD), and cellulose hybridized zeolitic diatomite (C/ZD)). The study involved the detection of the impact of the different modification steps on the adsorption properties of the obtained structures in terms of the adsorbent/adsorbate interface. This was accomplished based on the experimental factors and the mathematical parameters that were obtained from advanced equilibrium modeling according to statistical physics theory.

2 Experimental work

2.1. Materials

Purified natural diatomite powder (97.87% SiO_2) was obtained as a refined product from the Central Metallurgical and Development Institute in Egypt. The diatomite precursor was chemically refined by acid-washing processes using hydrochloric acid (37% purity) and hydrogen peroxide (30% purity) to get rid of metallic, carbonaceous, and carbonate impurities (Cornel Lab Company; Egypt). $Al(OH)_3$ (Sigma-Aldrich; Egypt) and NaOH pellets (97% purity; Sigma-Aldrich; Egypt) were incorporated during the zeolitization reactions of diatomite. Microcrystalline cellulose fibers (analytical grade) and dimethyl sulfoxide (DMSO) (CAS: 67-68-5; >99.5%; Sigma-Aldrich) were used during the facile functionalization of zeolitized diatomite with cellulose. Cadmium standard stock solution (1000 mg L; Sigma-Aldrich; Egypt) was used during the preparation of the polluted solutions at certain concentrations.

2.2. Synthesis of zeolitized diatomite (ZD)

Prior to the zeolitization process, the diatomite precursor (4 g) was incorporated into an acid washing step for 4 h using diluted HCL (10%), and this step was followed by another leaching process using H_2O_2 to ensure the effective removal of the associated impurities and obtain a high-purity product. The chemically purified product was incorporated into the alkaline hydrothermal zeolitization process. The diatomite powder was mixed with $Al(OH)_3$ within 100 mL of NaOH solution by a magnetic stirrer for 120 min at a certain speed (1000 rpm) and temperature (50 °C). The components of the mixture were incorporated at certain molar ratios (Si/Al (1 : 1.3), Na_2O/SiO_2

(1.4 : 1), and H$_2$O/Na$_2$O (40 : 1)). Afterward, the mixtures were transferred carefully into a Teflon-lined stainless steel autoclave (150 mL) as a conversion system and thermally treated at 120 °C for 5 h. Then, the synthetic zeolitized diatomite particles were extracted from the remaining alkaline solution, washed and neutralized with distilled water, and finally dried overnight at 85 °C.

2.3. Synthesis of cellulose fibers/zeolitized diatomite (C/ZD)

The functionalization of the obtained zeolite product with the cellulose fibers was performed based on the reported method by Altoom *et al.*,[35] 2 g of the produced ZD particulates were thoroughly homogenized in distilled water (50 mL) for 120 minutes, utilizing a sophisticated mixing apparatus that included a magnetic stirrer (500 rpm) and an ultrasound source (240 W). In a parallel procedure, 1 g of cellulose particles were disseminated in 50 mL of the DMSO solvent for 24 hours *via* stirring at 500 rpm, followed by a 120 minutes sonication. The resultant cellulose suspension was blended continuously for 24 hours with the previously produced ZD suspension employing a magnetic stirrer that rotated at 500 rpm and ultrasound radiation of 240 W. The produced C/ZD particulates were subsequently recovered from the remaining solution *via* a centrifugation process for 15 minutes at 3500 rpm, rinsed repeatedly with water to neutralize their surface, and afterward dried for 24 hours at 60 °C.

2.4. Analytical techniques

A Panalytical-Empyrean X-ray diffractometer was used to acquire X-ray patterns with a measurement range from 0 to 70°, which were used to identify the crystal phases in addition to their structural parameters. The key chemical groups, in addition to all of the incorporated groups throughout the functionalization phases, were detected utilizing a Fourier Transform Infrared spectrometer (FTIR8400S; Shimadzu) within an estimated range of 400 cm^{-1} to 4000 cm^{-1}. On the basis of photos of synthetic products obtained with a scanning electron microscope (Gemini, Zeiss Ultra 55), the surface morphologies and alterations as a result of modification processes have been investigated. A surface area analyzer (Beckman Coulter SA3100) was used to measure the porosity and surface area in accordance with the N$_2$ adsorption/desorption isotherm curves that have been obtained from the raw and hybridized materials.

2.5. Adsorption studies

The adsorption of Cd(II) by C/ZD in comparison with ZD and DA was completed in batch mode, implementing the experimental impact of the important variables, including the pH (2 to 7), adsorption duration (60 to 1440 min), and Cd(II) concentrations (50 to 400 mg L^{-1}) in light of the variation in the adjusted retention temperature from 293 K until 313 K. Moreover, the dosages of the diatomite-based adsorbents and the volumes of the Cd(II) solutions were fixed at 0.2 g L^{-1} and 200 mL, respectively. Each of these adsorption tests was carried out three times, and the average findings were utilized to depict the

data. The remaining Cd(II) concentrations after the desorption experiments were measured after acidification of the solutions with diluted nitric acid using inductively coupled plasma mass spectrometry (PerkinElmer). The measurements were conducted in the presence of a reference standard solution, which was documented by Merck Company (Germany) and the National Standard and Technology Institute (NIST). The measured concentrations of the remaining Cd(II) were used to calculate the actual or experimental Cd(II) adsorption capacity (Q_e) according to eqn (1), where C_o, C_e, V, and m are the tested Cd(II) concentration (mg L^{-1}), the remaining Cd(II) concentration (mg L^{-1}), the volume (mL), and the incorporated adsorbent dosage (mg).

$$Q_{e(\text{mg g}^{-1})} = \frac{(C_o - C_e)V}{m} \tag{1}$$

The kinetic and traditional isotherm properties of the Cd(II) adsorption processes by DA, ZD, and C/ZD were pursued in accordance with the non-linear fitting results of the illustrative equations of the models, which were assessed based on the determination coefficient (R^2) (eqn (2)) and Chi-squared (χ^2) (eqn (3)). Regarding the advanced isotherm investigations depending upon the specified models according to the statistical physics theory, the non-linear fitting degrees were evaluated based on the determination coefficient (R^2) in addition to the root mean square error (RMSE) (eqn (4)). The m', p, Qi$_{cal}$, and Qi$_{exp}$ symbols in the equation identify the inserted data, adsorption experimental variables, theoretical Cd(II) uptake capacity, and experimental Cd(II) uptake capacity, respectively.

$$R^2 = 1 - \frac{\sum \left(Q_{e,\text{exp}} - Q_{e,\text{cal}}\right)^2}{\sum \left(Q_{e,\text{exp}} - Q_{e,\text{mean}}\right)^2} \tag{2}$$

$$\chi^2 = \sum \frac{\left(Q_{e,\text{exp}} - Q_{e,\text{cal}}\right)^2}{Q_{e,\text{cal}}} \tag{3}$$

$$\text{RMSE} = \sqrt{\frac{\sum_{i=1}^{m} \left(\text{Qi}_{cal} - \text{Qi}_{exp}\right)^2}{m' - p}} \tag{4}$$

3 Results and discussion

3.1. Characterization of the used adsorbents

The obtained XRD patterns were used to follow the phase transformation and functionalization processes. The incorporated diatomite frustules exhibit the known pattern of amorphous or opaline silica with its broad peak around the 2 Theta angle of 22° (Fig. 1A). The zeolitized diatomite (ZD) reflects the significant recrystallization of the diatomite siliceous structure into a highly crystalline synthetic zeolite phase, which involved synthetic sodalite (JCPDS # 01-071-53569) in addition to zeolite Na-A (ICCD ref. code no. 00-039-0222) (Fig. 1B). The observed pattern of the integrated cellulose fibers reflects its crystalline nature, with common peaks of commercial cellulose at 14.6°
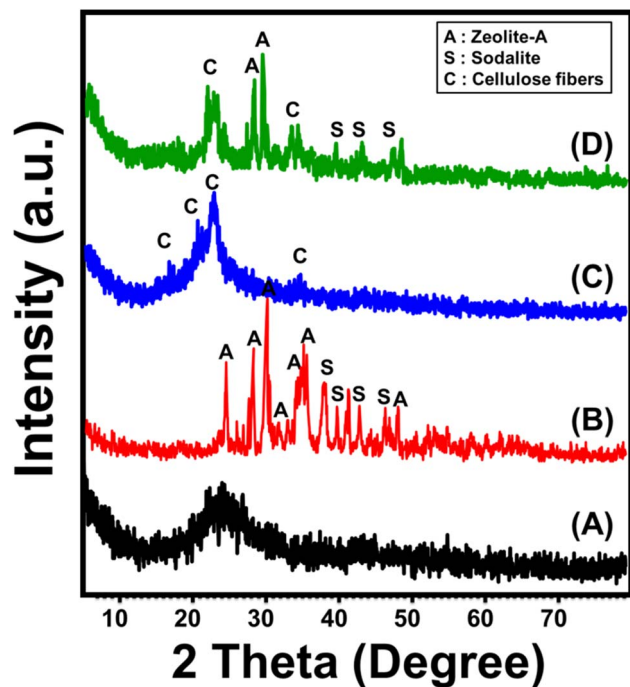
Fig. 1 XRD patterns of the raw diatomite (A), zeolitized diatomite (B), cellulose fibers (C), and C/ZD composite (D).

which deviated and their intensities declined at a considerable rate (Fig. 1D).

The SEM images were used to follow the change in morphology during the different modification steps. The raw samples display the known siliceous skeletons or frustules of diatoms that are characterized by highly porous pinnate forms (Fig. 2A). The SEM images of the zeolitized product show pinnate diatomite frustules to be coated with the synthetic zeolite phases, either the sodalite with its flower-like shape or zeolite-A with its cubic morphology (Fig. 2B–D). The orientation of the synthetic zeolite according to the outlines of the diatomite frustules and the detection of diatomite relicts suggested partial and non-extensive transformation of all the diatomite fractions into synthetic zeolite phases or the production of a zeolite/diatomite hybrid structure (Fig. 2B–D). Regarding the SEM images of the prepared C/ZD composite, the formed ZD particles appeared as decorated grains on the longitudinal or tabular surfaces of the cellulose fibers (Fig. 2E and F). This gives the final structure rugged topography and, in turn, enhanced surface area. The measured surface area values of DA, ZD, and C/ZD are 117.7 m^2 g^{-1}, 356 m^2 g^{-1}, and 372.4 m^2 g^{-1}, respectively.

The synthesis procedures were also followed based on the FT-IR spectra of D, ZD, and C/ZD (Fig. 3). The spectrum of diatomite demonstrates the existence of its characteristic active silanol groups (Si–O–H) at 3437 cm^{-1} in addition to symmetric (1092 cm^{-1}) and asymmetric (700 cm^{-1}) Si–O–Si and Si–O bond (465 cm^{-1}) (Fig. 3A).[24,29] The spectrum of the zeolitized sample confirms the existence of the essential functional groups of synthetic zeolite, such as Si–OH (3610 cm^{-1}), Al–OH (3427.4 cm^{-1}), zeolitic water (1471 cm^{-1}), Si–O–Si (992 cm^{-1}), Si–O (708 cm^{-1}), and Si–O–Al (551 cm^{-1}) (Fig. 3B).[34,44] The

(1 1̄ 0), 16.62° (110), 22.7° (200), and 34.6° (004) (JCPDS card no. 00-056-1718) (Fig. 1C). The observed XRD pattern of the zeolitized sample after functionalization with cellulose confirms the chemical interaction and integration between them (Fig. 1D). The characteristic peaks of cellulose were identified clearly in addition to the essential peaks of the formed zeolite phases,
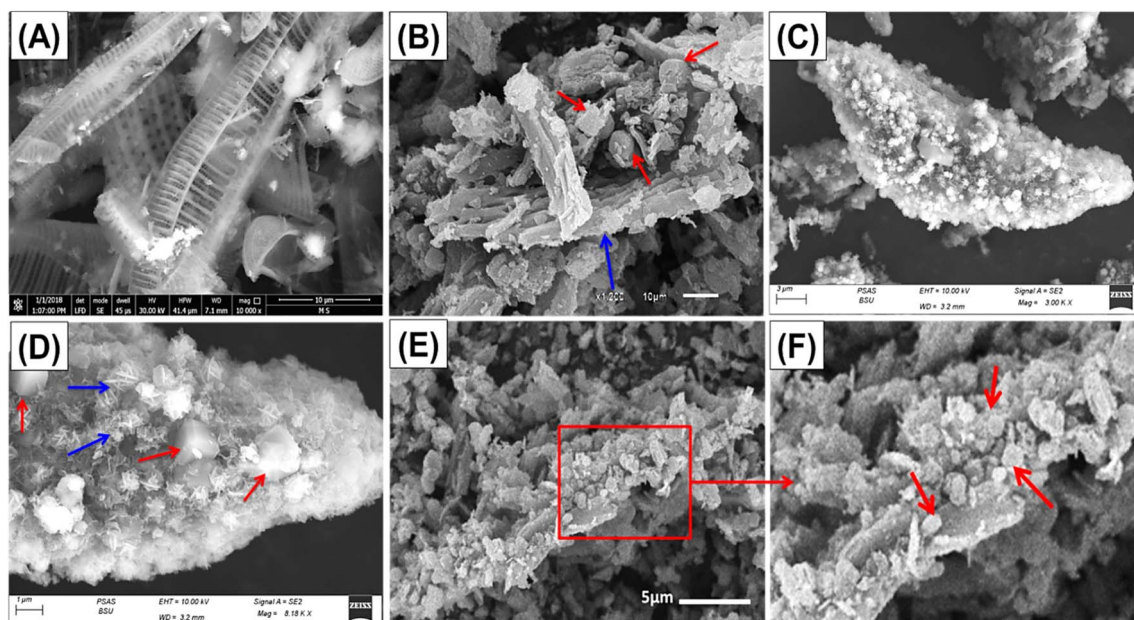

Fig. 2 SEM images of raw diatomite (A), zeolitized diatomite (red arrows refer to the synthetic zeolite and the blue arrow refers to the relicts of diatomite frustules) (B), zeolitized diatomite with the pinnate form of diatomite (C), the synthetic zeolite on the surface of diatomite (blue arrows refer to sodalite and red arrows refer to zeolite-A) (D), and the synthetic C/ZD composite (E and F).
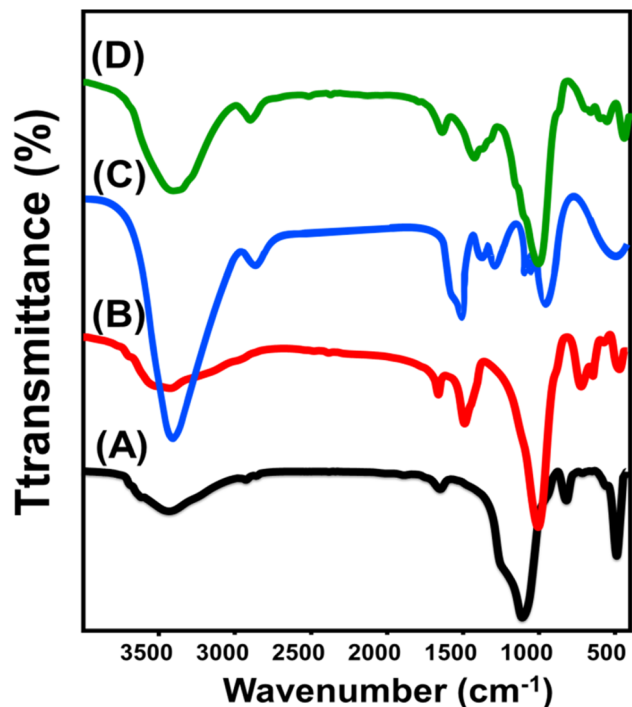
Fig. 3   FT–IR spectra of the raw diatomite (A), zeolitized diatomite (B), cellulose fibers (C), and C/ZD composite (D).

spectrum of the C/ZD composite was assessed in comparison with the spectrum of pure cellulose fibers. The spectrum of separated cellulose fibers demonstrates clearly the bands of the structural organic groups such as –CH-bearing chemical groups (2914 and 1367 cm^{-1}), –C–O–C bonds within the pyranose rings (1057 cm^{-1}), and the β-glycosidic linkages (897 cm^{-1}) (Fig. 3C).[21,35] The spectrum of C/ZD shows some bands related to the organic structure of cellulose as the –CH bearing functional groups (2902 and 1381 cm^{-1}) and other bands related to the silicate structure of zeolite (Si–O–Al (563 cm^{-1}), Si–O (670 cm^{-1}), Si–O–Si (1012 cm^{-1}), zeolitic water (1433 cm^{-1}), and Al–OH (3407 cm^{-1})) (Fig. 3D). The defection of such complex organic/inorganic structural chemical groups and the considerable deviation of their absorption bands validate the formation of a cellulose/zeolite hybrid structure with significant chemical interaction between their reactive chemical groups.

3.2.   Adsorption studies

3.2.1.   Effect of pH. The experimental or actual influence of the pH of the aqueous solutions on the uptake properties of DA, ZD, and C/ZD as potential adsorbents of Cd(II) was evaluated from pH 2 until pH 7 as the upper limit to avoid the expected precipitation of the hydroxide species at the higher pH conditions. All these tests were completed after careful adjustment of all the affecting parameters at fixed values [Cd(II) concentration: 100 mg L^{-1}; volume: 200 mL; time: 120 min; solid dosage: 0.2 g L^{-1}; temperature: 20 °C]. The actually determined Cd(II) adsorption capacities using DA, ZD, and C/ZD reveal notable enhancement in terms of the increase in the adjusted pH of the prepared aqueous solutions from pH 2 (6.3 mg g^{-1} (DA), 8.7 mg

Fig. 4   The experimental effect of the pH on the Cd(II) retention properties of DA, ZD, and C/ZD.

g^{-1} (ZD), and 14.5 mg g^{-1} (C/ZD)) until pH 7 (47.8 mg g^{-1} (DA), 50.7 mg g^{-1} (ZD), and 60.4 mg g^{-1} (C/ZD)) (Fig. 4). This experimental behavior at the different pH conditions validates the qualifications of DA as well as ZD and C/ZD as effective adsorbents during the realistic decontamination of the metal ions based on the recommended pH range of the industrial effluents by the US EPA (pH 6 to 9).[45] The reported actual enhancement can be illustrated based on both the speciation behaviors of Cd(II) as well as the surficial charges of DA, ZD, and C/ZD. According to the speciation curve of cadmium, it exists as positively charged Cd^{2+} cations within the evaluated pH range, and beyond pH 8, it precipitates in hydroxide form [Cd(H$_2$O$_6$)]$^{2+}$.[46] Moreover, the considerable de-protonation of the functional groups of DA, ZD, and C/ZD at higher pH conditions provides their surfaces with numerous negative charges, which accelerate the electrostatic attractions of Cd^{2+} cations.[4]
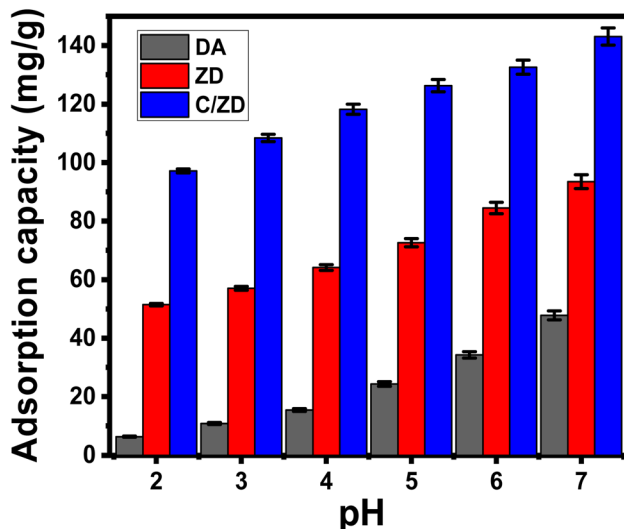
3.2.2.   Kinetic studies

3.2.2.1.   Effect of contact time. The experimental influence of the adsorption duration on the achieved capacities by DA, ZD, and C/ZD was followed within an evaluated range from 30 min until 1320 min at adjusted values of the main affecting parameters [Cd(II) concentration: 100 mg L^{-1}; volume: 200 mL; solid dosage: 0.2 g L^{-1}; pH: 7; temperature: 20 °C]. The retention properties of DA, ZD, and C/ZD as potential adsorbents of Cd(II) validate notable enhancement in terms of the observed rate as well as the adsorbed quantities in mg g^{-1} with the adjustable expanding of the testes duration (Fig. 5A). This actual enhancement influence can be observed up to 600 min in the presence of DA and up to 840 min in the presence of ZD and C/ZD particles. Afterward, the increase in the duration of the tests reveals no considerable influences either on the retention rates or adsorbed Cd(II) quantities, which demonstrate stability or equilibration states (Fig. 5A). During such states, the DA, ZD, and C/ZD particles exhibit their equilibrium adsorption capacities of Cd(II) (78.5 mg g^{-1} (DA), 97.6 mg g^{-1} (ZD), and 117.2 mg g^{-1} (C/ZD)) (Fig. 5A). The existence of the active adsorption sites
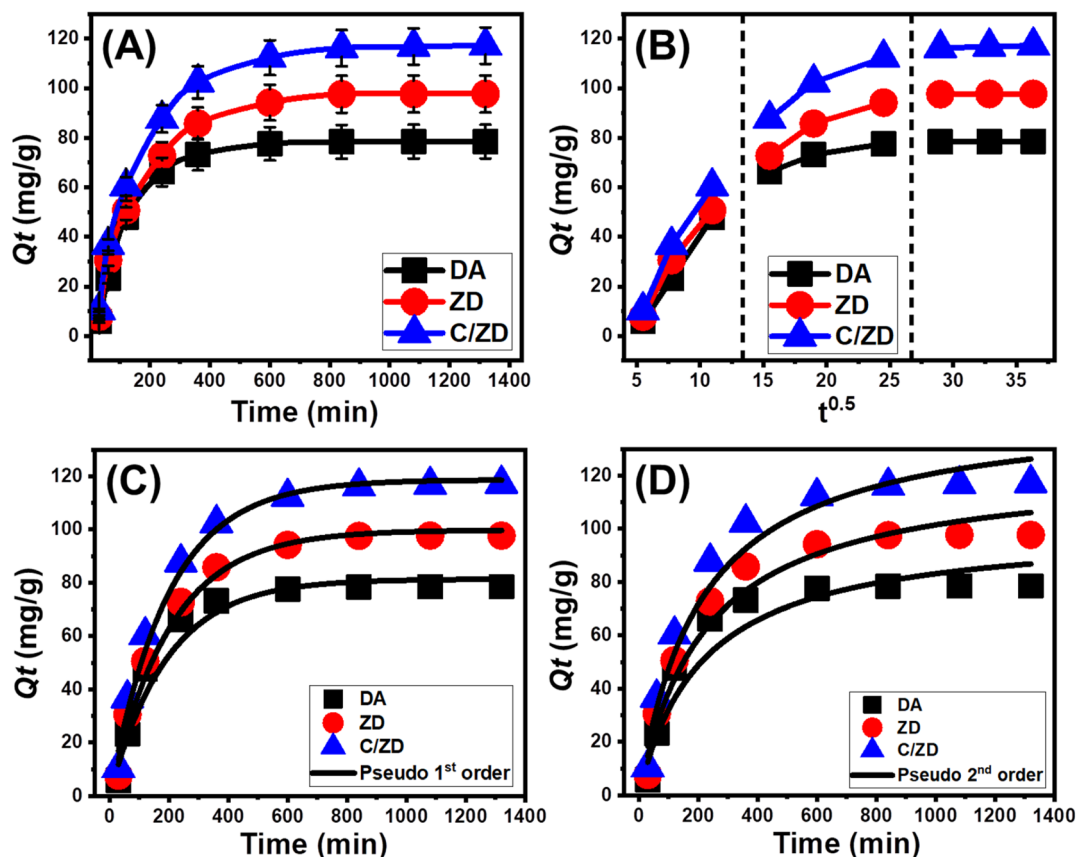
Fig. 5 Experimental effect of the Cd(II) uptake duration on the capacities of DA, ZD, and Z/ZD (A), the intra-particle diffusion curves of Cd(II) uptake processes by DA, ZD, and Z/ZD (B), fitting of the Cd(II) uptake processes with the Pseudo-first order kinetic model (C), and fitting of the Cd(II) uptake processes with the Pseudo-second order kinetic model (D).

at their free states and extensive quantities on the DA, ZD, and C/ZD particles at the starting intervals of the retention reactions resulted in the detected high rates and abrupt increase in the adsorbed Cd(II) quantities.[47] The progressive retention of Cd(II) in the existing free sites of DA, ZD, and C/ZD with the rising period of the tests causes occupation and consumption of these sites, which strongly declines their availability. Therefore, the experimental retention rates dropped clearly after certain time intervals, and the DA, ZD, and C/ZD showed no enhancement in their adsorption properties. The equilibration states of DA, ZD, and C/ZD were identified after the complete occupation of all the existing sites with the Cd(II) ions.[3]

3.2.2.2. Intra-particle diffusion behavior. For the adsorption of Cd(II) into DA, ZD, and C/ZD, three different stages of intra-particle diffusion curves with no crossovers with the curves' starting points have been found (Fig. 5B). This shows that the Cd(II) ions are kept in place by mechanisms that work together, and that the diffusion of ions towards the active receptors of DA, ZD, and C/ZD has a big effect.[48,49] This could be caused by (A) loading by the spread-out active sites on the outside surface (border), (B) diffusion within the particle, and (C) the impact of the equilibrium stages on the way things work.[50] The occurrence of the first stage denotes the activity of the exterior adsorption mechanisms during the initial stages of the experiments, and

the quantity of the surface-active receptors controls how effectively the adsorption reactions proceed (Fig. 5B).[6] By extending the retention period of Cd(II), a new stage has been observed (Fig. 5B) that denotes the existence of additional mechanisms, including the impact of the Cd(II) diffusion actions and the layered adsorption activities.[38,50] Finally, the equilibrium states of DA, ZD, and C/ZD during the Cd(II) retention reactions show the third stage to be the most predominant stage. This implies that the retention of Cd(II) ions has occupied or consumed all the efficient binding sites (Fig. 5B).[7,49] During this step, multiple mechanisms influence the adsorption reactions, which may involve molecular interaction as well as an interionic attraction.[46]

3.2.2.3. Kinetic modeling. The kinetic properties of the Cd(II) processes by DA, ZD, and C/ZD were illustrated according to the reported kinetic assumptions of Pseudo-first-order mode (P.F.) as well as Pseudo-second-order (P.S.) models. The agreement between the assumptions of these two models and the obtained Cd(II) uptake results was evaluated based on the recognized non-linear fitting degrees with the representative equations of these models depending on both the values of correlation coefficient (R^2) in addition to Chi-squared (χ^2) (Table 1; Fig. 5C and D). The determined values of R^2 in addition to χ^2 declared a higher fitting of Cd(II) adsorption reactions by DA, ZD, and C/

Table 1 The mathematical parameters of the addressed kinetic models

Material	Model	Parameters	293 K
		Kinetic models	
D	Pseudo-first-order	K_1 (1/min)	0.0052
		$Q_{e\,(Cal)}$ (mg g^{-1})	81.37
		R^2	0.95
		X^2	1.399
	Pseudo-second-order	k_2 (mg g^{-1} min^{-1})	4.65×10^{-5}
		$Q_{e\,(Cal)}$ (mg g^{-1})	100.83
		R^2	0.93
		X^2	2.24
ZD	Pseudo-first-order	K_1 (1/min)	0.0049
		$Q_{e\,(Cal)}$ (mg g^{-1})	99.80
		R^2	0.97
		X^2	0.94
	Pseudo-second-order	k_2 (mg g^{-1} min^{-1})	3.64×10^{-5}
		$Q_{e\,(Cal)}$ (mg g^{-1})	123.89
		R^2	0.95
		X^2	1.59
C/ZD	Pseudo-first-order	K_1 (1/min)	0.0051
		$Q_{e\,(Cal)}$ (mg g^{-1})	118.7
		R^2	0.98
		X^2	0.81
	Pseudo-second-order	k_2 (mg g^{-1} min^{-1})	3.28×10^{-5}
		$Q_{e\,(Cal)}$ (mg g^{-1})	146.16
		R^2	0.96
		X^2	1.49

ZD with the kinetic behaviors and basics of the P.F. model than the assessed P.S. model. Such fitting findings were supported by the remarkable agreement between the actual equilibrium capacities (78.5 mg g^{-1} (DA), 97.6 mg g^{-1} (ZD), and 117.2 mg g^{-1} (C/ZD)) and the theoretically estimated capacities (81.3 mg g^{-1} (DA), 99.8 mg g^{-1} (ZD), and 118.7 mg g^{-1} (C/ZD)) (Table 1). According to the kinetic basics of the P.F. model, the retention of Cd(II) by DA, ZD, and C/ZD occurred predominantly by physical mechanisms that might include the remarkable influences of van der Waals forces as well as electrostatic attractions.[51,52] However, the retention of Cd(II) by DA, ZD, and C/ZD is highly fitted with the equation of the P.F. model as compared to the illustrative equation of the P.S. model, and the retention reactions still display high agreement with the P.S. kinetics. Therefore, an assistant or minor impact effect of some of the common weak chemical processes was expected during the reactions, such as hydrogen bonding, electron sharing, hydrophobic interactions, and chemical complexes.[49,51] The cooperation of both physical and chemical mechanisms involved the formation of a chemically adsorbed Cd(II) layer followed by the formation of a physically adsorbed layer using the first layer as substrate.[53]

3.2.3. Equilibrium studies

3.2.3.1. Effect of Cd(II) concentrations. After carefully setting all the affecting parameters at fixed values [volume: 200 mL; pH: 7; time: 24 h; solid dosage: 0.2 g L^{-1}; temperature: (293 K, 303 K, and 313 K)]; the effect of the initial Cd(II) concentration on the adsorption properties of DA, ZD, and C/ZD was studied over an experimental range of 50–400 mg L^{-1}. The initially tested

concentration is an effective parameter during the assessment of the adsorption properties of DA, ZD, and C/ZD to describe their equilibrium properties and their maximum capacities (Fig. 6A). Experimentally, the adsorbed quantities of Cd(II) by DA, ZD, and C/ZD increased notably after testing their properties in the presence of higher concentrations of the metal ions (Fig. 6A–C). The high concentration of Cd(II) in certain volumes causes a remarkable increase in the diffusion, mobility, and driving forces of its dissolved ions, which prompt their collision and chemical interaction with the distributed active sites on the surfaces of DA, ZD, and C/ZD and, in turn, the uptake efficiency.[46,49] The increase in the adsorbed quantities of Cd(II) in terms of the initially tested concentrations of its ions can be detected clearly up to certain studied concentrations (Fig. 6A–C). After that, the increase in the starting Cd(II) concentrations demonstrates a neglected effect on the adsorbed quantities of its ions by DA, ZD, and C/ZD, which identify their equilibrium states and the reorganization of their actual maximum uptake capacities. The equilibrium in the presence of DA can be identified after 300 mg L^{-1} at 313 K and after 250 mg L^{-1} at 293 and 303 K, achieving retention capacities of 128 mg g^{-1} (293 K), 111.5 mg g^{-1} (303 K), and 96.4 mg g^{-1} (313 K) (Fig. 6A). In the presence of ZD, equilibrium can be identified after 300 mg L^{-1} for all the addressed temperature values, achieving retention capacities of 178.6 mg g^{-1} (293 K), 157 mg g^{-1} (303 K), and 135.2 mg g^{-1} (313 K) (Fig. 6B). Regarding the synthetic C/ZD, equilibrium can also be detected after 300 mg L^{-1}, achieving a retention capacity of 220.6 mg g^{-1} (293 K), 186.6 mg g^{-1} (303 K), and 167.3 mg g^{-1} (313 K) (Fig. 6C). The remarkable high retention properties of C/ZD in comparison with DA and ZD might be related to (1) the enhanced surface area and (2) the remarkable increase in the quantity of effective sites after the integration of the cellulose chains. Also, the enhanced properties of ZD as compared to DA were attributed to the remarkable enhancement in the ion exchange capacity, surface reactivity, and surface area after the zeolitization processes. The observable diminution in the uptake of Cd(II) by DA, ZD, and C/ZD in terms of the temperature of the tests declared the exothermic nature of the reactions that occurred.

3.2.3.2. Giles's classification. The classification of the Cd(II) isotherm curves using DA, ZD, and C/ZD according to the reported criteria of Giles's classification demonstrates their formation in the L-type isotherm curves[54] (Fig. 6A–C). The L-type isotherm properties contribute to the remarkable and strong effects of the intermolecular attractive forces during the retention processes of Cd(II) by the DA, ZD, and C/ZD particles, in addition to the strong interaction between the metal ions and the reactive chemical groups of the previously mentioned adsorbents.[55] Additionally, the L-type isotherm properties theoretically suggested the complete formation of adsorbed Cd(II) monolayers on the surfaces of DA, ZD, and C/ZD particles.[56] Additionally, this isothermal behavior validates the enrichment of the DA, ZD, and C/ZD particles with numerous active and free adsorption receptors that are characterized by strong affinities to the Cd(II) ions during their adsorption, especially at low initial concentrations.
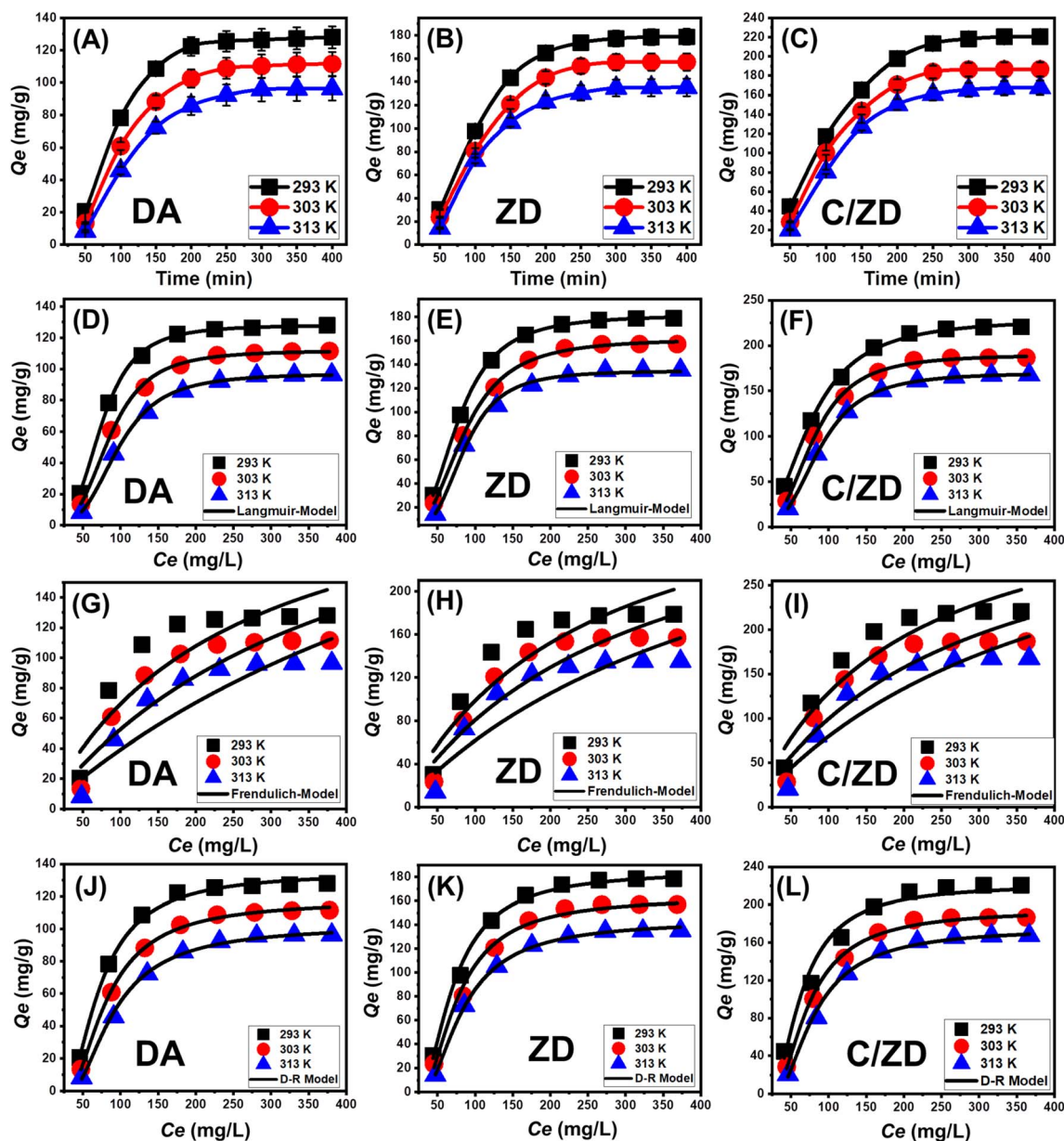
Fig. 6 Experimental effect of the Cd(II) concentration on the capacities of DA, ZD, and C/ZD (A–C), fitting of the Cd(II) uptake processes with Langmuir model (D–F), fitting of the Cd(II) uptake processes with Freundlich model (G–I), and fitting of the Cd(II) uptake processes with D-R model (J–L).

3.2.3.3. Classic isotherm models. The equilibrium behaviors of the Cd(II) retention processes by the DA, ZD, and C/ZD particles were described according to the isotherm assumptions of classic Langmuir, Freundlich, and Dubinin-Radushkevich (D-R) models. The agreement between the assumptions of these two models and the obtained Cd(II) uptake results was evaluated based on the recognized non-linear fitting degrees with the representative equations of these models depending on both the values of correlation coefficient (R^2) in addition to Chi-squared (χ^2) (Table 2; Fig. 6). The values of R^2 and χ^2 declared the higher fitting of the Cd(II) retention processes by the DA, ZD, and C/ZD particles with isotherm basics of Langmuir assumption (Fig. 6D–F; Table 2)

than the reported properties of Freundlich isotherm (Fig. 6G–I; Table 2). The Langmuir isotherm system donates the retention of Cd(II) homogenously by the free sites of DA, ZD, and C/ZD particles in monolayer forms.[51,52] Moreover, the estimated RL parameter of the Cd(II) retention processes by the DA, ZD, and C/ZD particles exhibits a value <1, signifying the favorable nature of the uptake processes.[6,7] As an estimated parameter of Langmuir modeling, the expected maximum Cd(II) uptake capacities (Qe_{max}) at the best experimental temperature (392 K) by DA, ZD, and C/ZD are 128.13 mg g^{-1}, 181.4 mg g^{-1}, and 229.6 mg g^{-1}, respectively.

The isotherm properties of the D-R model (Fig. 6J–L) signify notably the energetic heterogeneities of the DA, ZD, and C/ZD

Table 2 The mathematical parameters of the addressed classic isotherm models

Materials	Models		293 K	303 K	313 K
DA	Langmuir model	Q_{max} (mg g^{-1})	128.13	111.8	97
		b (L mg^{-1})	4.4×10^{-7}	3.49×10^{-7}	1.93×10^{-7}
		R^2	0.99	0.99	0.99
		X^2	0.012	0.037	0.033
	Freundlich model	$1/n$	0.75	0.70	0.68
		k_F (mg g^{-1})	0.61	0.55	0.47
		R^2	0.63	0.75	0.82
		X^2	4.1	3.2	2.3
	D-R model	β (mol^2 kJ^{-2})	1.60	2.01	2.5
		Q_m (mg g^{-1})	134.76	117.42	101.91
		R^2	0.99	0.99	0.99
		X^2	0.05	0.02	0.04
		E (kJ mol^{-1})	0.55	0.49	0.44
ZD	Langmuir model	Q_{max} (mg g^{-1})	181.4	161.3	134.6
		b (L mg^{-1})	3.33×10^{-6}	3.26×10^{-6}	1.39×10^{-7}
		R^2	0.99	0.99	0.99
		X^2	0.002	0.019	0.115
	Freundlich model	$1/n$	0.82	0.79	0.76
		k_F (mg g^{-1})	0.80	0.72	0.62
		R^2	0.65	0.72	0.77
		X^2	3.66	3.32	2.65
	D-R model	β (mol^2 kJ^{-2})	1.5	1.75	2.08
		Q_m (mg g^{-1})	185.02	163.1	143.31
		R^2	0.997	0.994	0.999
		X^2	0.13	0.25	0.02
		E (kJ mol^{-1})	0.57	0.53	0.49
C/ZD	Langmuir model	Q_{max} (mg g^{-1})	229.6	189.9	170.01
		b (L mg^{-1})	4.16×10^{-5}	2.38×10^{-6}	9.67×10^{-7}
		R^2	0.99	0.99	0.99
		X^2	0.041	0.072	0.02
	Freundlich model	$1/n$	0.92	0.84	0.80
		k_F (mg g^{-1})	0.91	0.82	0.75
		R^2	0.60	0.69	0.77
		X^2	3.76	3.41	2.16
	D-R model	β (mol^2 kJ^{-2})	1.23	1.60	1.98
		Q_m (mg g^{-1})	221.53	194.43	175.11
		R^2	0.98	0.99	0.99
		X^2	0.77	0.12	0.18
		E (kJ mol^{-1})	0.63	0.55	0.50

particles during their adsorption for the Cd(II) ions regardless of the nature of their surfaces, whether heterogeneous or homogenous.[57] The value of Gaussian energy (E) as a mathematical parameter from the D-R modeling process considerably validates the type of the affecting Cd(II) retention mechanisms (chemical or physical). The retention reactions that exhibit E values <8 kJ mol^{-1}, from 8 to 16 kJ mol^{-1}, and >16 kJ mol^{-1} signify the effects of strong physical, weak chemical, complex physical/chemical, and strong chemical properties, respectively.[7,57] The values of the E parameter of the Cd(II) retention processes either by DA or its modified products of ZD and C/ZD are within the reported energy values of physical processes (<8 kJ mol^{-1}) but also within the signified range of zeolitic ion exchange mechanisms (0.6–25 kJ mol^{-1}), which match the theoretical findings of the kinetic studies (Table 1).

3.2.3.4. Advanced isotherm modeling. The recently studied advanced isotherm models, according to the hypothesis of the statistical physics theory, can strongly signify the nature of the adsorption reactions in terms of the adsorbent/adsorbate interface and the surficial properties of the solid adsorbents. These scientific implications can be illustrated based on the associated mathematical parameters of these models, including the steric parameters and the energetic parameters. The steric parameters involved the occupied active site density of DA, ZD, and C/ZD ($N_{m(Cd(II))}$), number of adsorbed Cd(II) ions per each site ($n_{(Cd(II))}$), their adsorption capacities during the saturation states (Q_{sat}). The energetic parameters involved the retention energy of Cd(II) (ΔE) and the internal energy of the adsorption systems (E_{int}) in addition to the free enthalpy (G), and entropy (S_a). The modeling of the Cd(II) retention reactions was performed based on the non-linear fitting of the representative equations of these models. This was accomplished by the Levenberg–Marquardt iterating algorithm as a function of multivariable nonlinear regression. A monolayer model with one energy site was selected to illustrate the adsorption reactions of Cd(II) by DA, ZD, and C/ZD considering the fitting degrees (Fig. 7A–C; Table 3).
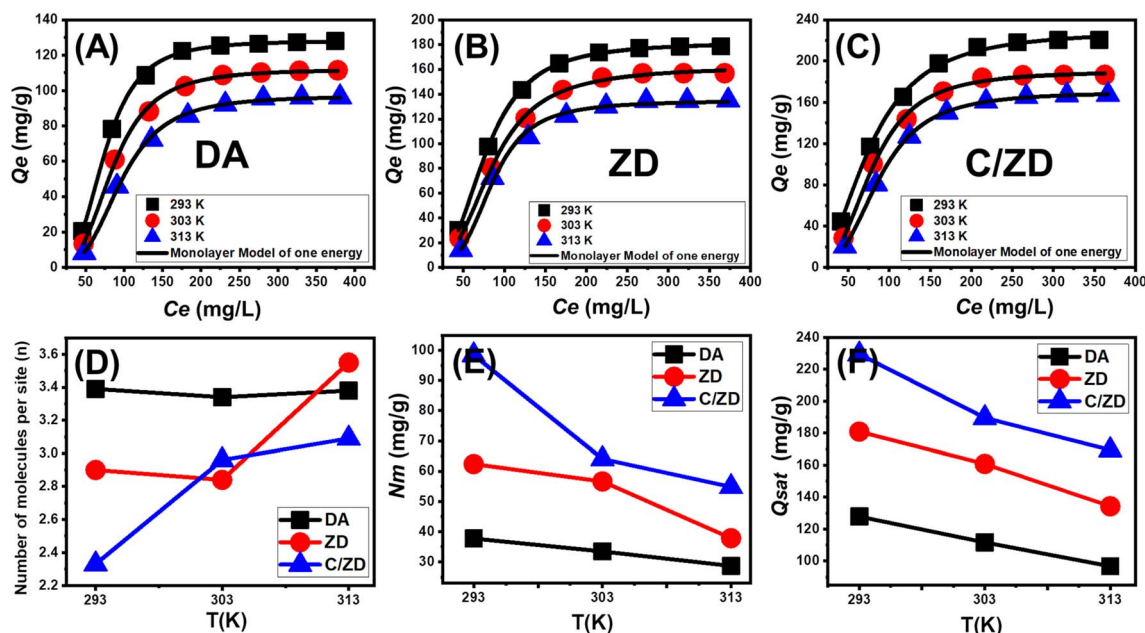
Fig. 7 Fitting of the Cd(II) uptake processes with advanced monolayer model of one energy site (A–C), the changes in the numbers of adsorbed Cd(II) with temperature (D), the changes in the active sites density during the uptake of Cd(II) with temperature (E), and the changes in the adsorption capacities of Cd(II) with temperature during the saturation states of DA, ZD, and C/ZD (F).

3.2.3.5. Steric properties. 3.2.3.6. Number of adsorbed Cd(II) (n) per each site. The values of the $n_{(Cd(II))}$ parameter strongly signify the orientation of the adsorbed Cd(II) ions on the surfaces of the DA, ZD, and C/ZD (vertical or horizontal) in addition to their significance about the affecting mechanisms (multi-docking or multi-interactions). The retention systems of the metal ions that display values <1 are associated with the horizontal orientation of the adsorbed ions, and the reactions are affected mainly by multi-anchorage or multi-docking mechanisms involving the adsorption of one metal by several active free sites. Conversely, the systems that display values >1 are associated with the non-parallel and vertical orientation of the adsorbed ions, and the reactions are affected mainly by multi-ionic mechanisms involving the adsorption of more than one metal ion per only one active free site.[7,58] The determined values of $n_{(Cd(II))}$ during the uptake of Cd(II) by DA (n = 3.34–

3.39), ZD (n = 2.9–3.55), and C/ZD (n = 2.33–3.09) are higher than 1 (Fig. 7D; Table 3). Therefore, the Cd(II) ions were absorbed by multi-ionic processes during which each active site of DA, ZD, and C/ZD can adsorb about 4 ions in vertical orientations.

Regarding the impact of the temperature, the determined $n_{(Cd(II))}$ values of the composite C/ZD validate an increase in terms of the increase in the temperature from 293 K until 313 K (Fig. 7D). This was commonly assigned to the predicted increase in the aggregation properties of Cd(II) during their retention on the surface of C/ZD at high adsorption conditions.[34] Moreover, this reflects the occurrence of thermal (energetic) activation processes before the retention of Cd(II) by C/ZD.[2,59] For both DA and ZD, the values decline within the temperature range from 293 K until 303 K and then increase again within the temperature range from 303 K until 313 K (Fig. 7D). This behavior

Table 3 The mathematical parameters of the addressed advanced equilibrium model (monolayer model of one energy)

Steric and energetic parameters

		n	N_m (mg g⁻¹)	Q_{sat} (mg g⁻¹)	$C_{1/2}$ (mg L⁻¹)	ΔE (kJ mol⁻¹)
D	293 K	3.39	37.72	127.87	74.43	−5.97
	303 K	3.34	33.43	111.65	85.05	−6.05
	313 K	3.38	28.63	96.76	95.87	−6.13
ZD	293 K	2.90	62.37	180.873	76.35	−5.95
	303 K	2.84	56.62	160.80	84.14	−6.06
	313 K	3.55	37.83	134.29	84.53	−6.25
C/ZD	293 K	2.33	98.46	229.41	75.56	−5.96
	303 K	2.96	64.04	189.55	78.66	−6.12
	313 K	3.09	54.84	169.45	87.11	−6.22

suggested changes in the quantities and nature of the dominant active sites on the surfaces of D and ZD with the changes in the adjusted temperature of the retention reactions.[38,60]

3.2.3.7. Occupied active sites density (N_m). The density of the occupied active sites (N_m) signifies strongly the quantities of the present free and effective adsorption sites on the surfaces of DA, ZD, and C/ZD during their retention of Cd(II) ions (Fig. 7E; Table 3). The estimated $N_{m(Cd(II))}$ values of DA are 37.7 mg g^{-1} (293 K), 33.4 mg g^{-1} (303 K), and 28.6 mg g^{-1} (313 K). For ZD, the Nm$_{(Cd(II))}$ values increased to 62.37 mg g^{-1} (293 K), 56.6 mg g^{-1} (303 K), and 37.8 mg g^{-1} (313 K). After the cellulose functionalization process, the estimated $N_{m(Cd(II))}$ values of the composite enhanced greatly to 98.4 mg g^{-1} (293 K), 64 mg g^{-1} (303 K), and 54.8 mg g^{-1} (313 K). The results declared a significant increase in the quantities of the active sites after the zeolitization process, which might be assigned to the effect of the ion exchange processes within the zeolite structure. Moreover, the reported enhancement in the surface area and the existence of numerous structural nanopores provide additional interaction interfaces between the Cd(II) ions and other active sites. This enhancement was notably increased after the hybridization process of the ZD particles with cellulose fibers. This occurred as a result of the integration of new active sites related to the functional groups of cellulose, in addition to the reported increase in surface area, which enhances the interaction surface with the ions in the solution. Regarding the temperature effect on the $N_{m(Cd(II))}$ values of DA, ZD, and C/ZD exhibit reversible relations with the temperature (Fig. 7E; Table 3). This is in agreement with the previously recognized values of $n_{(Cd(II))}$ as the increase in the aggregation affinity reduces the quantities of the occupied active adsorption sites.[2,61]

3.2.3.8. Adsorption capacity at the saturation state of (Q_{sat}). The Cd(II) adsorption capacities of DA, ZD, and C/ZD at their saturation states (Q_{sat}) are the most likely values for their maximum capacities. The values of Q_{sat} are controlled by two essential factors: the quantities of the present active sites ($N_{m(Cd(II))}$) and the numbers of the adsorbed Cd(II) ions per each site ($n_{(Cd(II))}$). The estimated Q_{sat} values of DA as an adsorbent of Cd(II) are 127.8 mg g^{-1} (293 K), 111.6 mg g^{-1} (303 K), and 96.6 mg g^{-1} (313 K) while the estimated values for ZD are 180.8 mg g^{-1} (293 K), 160.8 mg g^{-1} (303 K), and 134.29 mg g^{-1} (313 K) (Fig. 7F; Table 3). For C/ZD, the estimated Q_{sat} values are 229.4 mg g^{-1} (293 K), 189.5 mg g^{-1} (303 K), and 169.4 mg g^{-1} (313 K). The adverse effect of the temperature affects the exothermic properties of the Cd(II) uptake reactions by DA, ZD, and C/ZD (Fig. 7F; Table 3). Also, this marked the acceleration impact of the uptake temperature on the thermal collisions, which causes a reduction in the adsorption efficiency.[58] Moreover, the determined behaviors of Q_{sat} as a function of the uptake temperature match the reported behaviors of $N_{m(Cd(II))}$ rather than $n_{(Cd(II))}$ demonstrating the controlling effect of the present active sites on the adsorption efficiency rather than the capacity of each active site.

3.2.3.9. Energetic properties. 3.2.3.10. Adsorption energy. The energies (ΔE) of the Cd(II) retention reactions can effectively demonstrate the nature of the affecting mechanisms, either physical or chemical processes. The chemical mechanisms exhibit energy values higher than 80 kJ mol^{-1}, while the affecting physical mechanisms exhibit energy values ≤40 kJ mol^{-1}. The physical mechanisms are also classified into different types based on the adsorption energy values involving (1) coordination exchange (40 kJ mol^{-1}), (2) hydrogen bonding (<30 kJ mol^{-1}), (3) dipole forces (2 to 29 kJ mol^{-1}), (4) van der Waals forces (4 to 10 kJ mol^{-1}), and (5) hydrophobic bonds (5 kJ mol^{-1}).[34,62,63] The values of the Cd(II) retention energy (ΔE) were obtained theoretically from eqn (1) based on the solubility of cadmium in water (S), gas constant ($R = 0.008314$ kJ mol^{-1} K^{-1}), absolute temperature (T), and the concentration of Cd(II) at the half saturation states of DA, ZD, and C/ZD.[60]

$$\Delta E = RT \ln\left(\frac{S}{C}\right) \quad (5)$$

The retention of Cd(II) by DA exhibits energy values within the range from −5.9 to −6.13 kJ mol^{-1}, and for the reactions that occurred by ZD, the detected retention energies are −5.95 kJ mol^{-1} (293 K), −6.06 kJ mol^{-1} (303 K), and −6.25 kJ mol^{-1} (313 K) (Table 3). Also, the application of C/ZD composite as an adsorbent for Cd(II) displays values within the previously reported ranges of DA and ZD (−5.96 to −6.22) (Table 3). Therefore, the retention of Cd(II) by DA, ZD, and C/ZD occurred predominantly by physical processes that might be involved in van der Waals forces (4 to 10 kJ mol^{-1}), hydrophobic bonds (5 kJ mol^{-1}), dipole forces (2 to 29 kJ mol^{-1}), and hydrogen bonding (<30 kJ mol^{-1}). Furthermore, the marked negative signs of the estimated values of ΔE during the retention of Cd(II) by DA, ZD, and C/ZD confirm the previously reported experimental findings about the exothermic properties of the reactions.

3.2.3.11. Thermodynamic functions. 3.2.3.12. Entropy. The entropy (S_a) of the Cd(II) retention processes by DA, ZD, and C/ZD significantly reflect the order and disorder properties of their surfaces in the presence of different concentrations of the metal ions as well as the temperature at which the reactions were conducted. The S_a behaviors were illustrated based on the obtained values from eqn (6), considering the concentration of Cd(II) at the half saturation states of DA, ZD, and C/ZD ($C_{1/2}$) as well as the previously obtained values of $N_{m(Cd(II))}$ and $n_{(Cd(II))}$.[60]

$$\frac{S_a}{K_B} = N_m\left\{\ln\left(1+\left(\frac{C}{C_{\frac{1}{2}}}\right)^n\right) - n\left(\frac{C}{C_{\frac{1}{2}}}\right)^n \frac{\ln\left(\frac{C}{C_{\frac{1}{2}}}\right)}{1+\left(\frac{C}{C_{\frac{1}{2}}}\right)^n}\right\} \quad (6)$$

Based on the obtained curves, the values of the entropy (S_a) during the retention of Cd(II) by Da, ZD, and C/ZD decrease notably for the conducted tests in the presence of high metal concentrations (Fig. 8A–C). This behavior demonstrates the
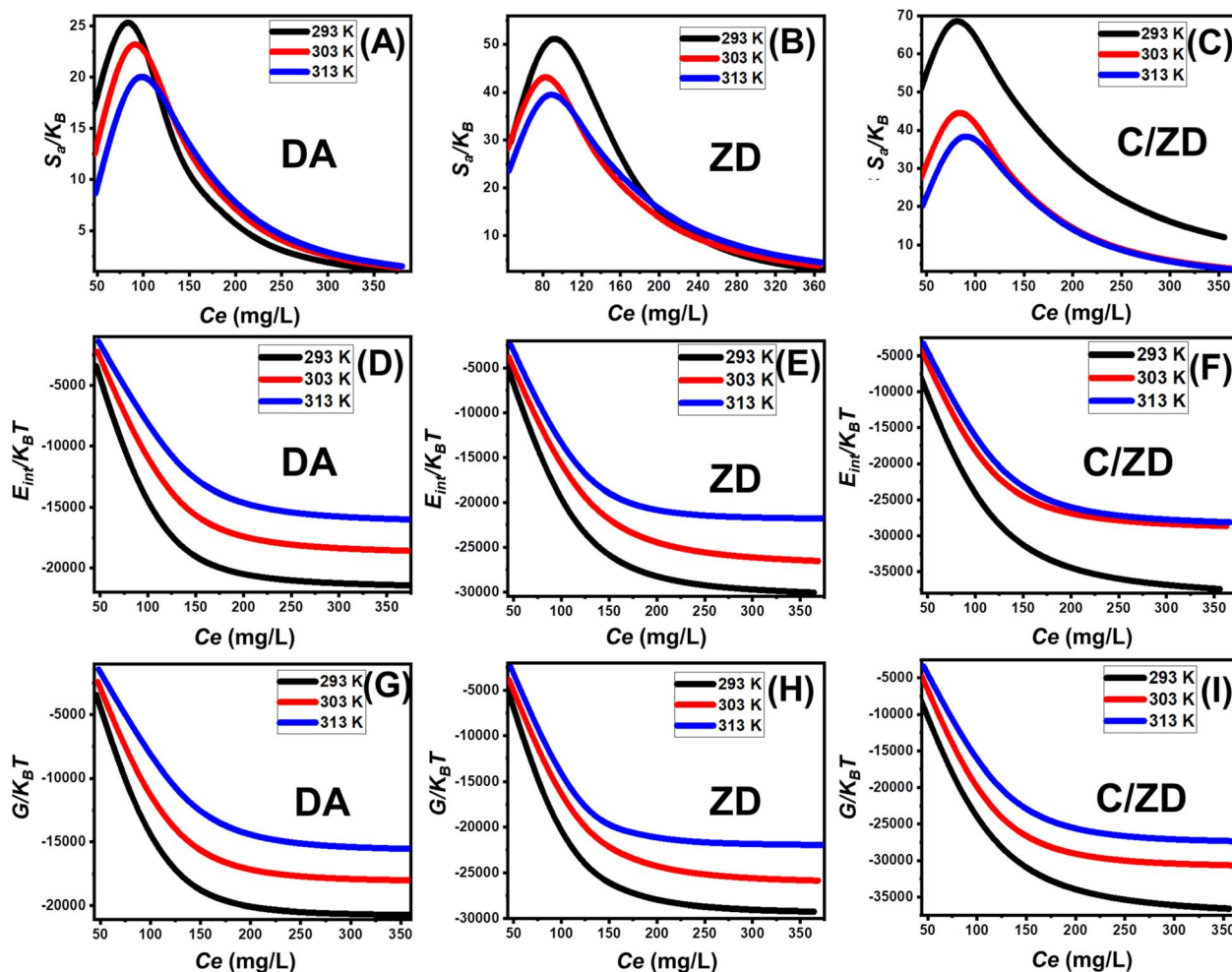
Fig. 8 The changes in the entropy during the uptake of Cd(II) with temperature (A–C), t the changes in the internal energy during the uptake of Cd(II) with temperature (D–F), and the changes in the free enthalpy during the uptake of Cd(II) with temperature (G–I).

remarkable declination in the disorder properties of the surfaces of DA, ZD, and C/ZD with the increase in the tested concentrations of Cd(II). Moreover, these entropy properties validate the effective docking of the Cd(II) ions into the present free and active adsorption receptors of DA, ZD, and C/ZD in the presence of low concentrations of the metal.[59,61] The maximum values of entropy during the retention of Cd(II) by DA were reported at corresponding equilibrium concentrations equal to 84.3 mg L^{-1} (293 K), 87.8 mg L^{-1} (303 K), and 90.8 mg L^{-1} (313 K). For ZD, the recognized equilibrium concentrations are 85.5 mg L^{-1} (293 K), 83.8 mg L^{-1} (303 K), and 80.4 mg L^{-1} (313 K). For C/ZD, the equilibrium concentrations of 76.5 mg L^{-1} (293 K), 79.9 mg L^{-1} (303 K), and 83.8 mg L^{-1} (313 K) were detected as the corresponding concentrations of the maximum entropy. These Cd(II) equilibrium concentrations are close to the estimated concentrations at the half saturation states of DA, ZD, and C/ZD. Therefore, the docking of additional Cd(II) ions on the free sites of DA, ZD, and C/ZD cannot occur. Additionally, the remarkable declines in the obtained values of entropy suggested a significant reduction in the diffusion properties of Cd(II) ions as well as their freedom degrees, in addition to

a strong diminution in the availability of the free adsorption sites.[63]

3.2.3.13. Internal energy and free enthalpy. The internal energy (E_{int}) of the Cd(II) uptake processes by DA, ZD, and C/ZD and the free enthalpy (G) properties and their behaviors in terms of the changes in the metal concentration and the uptake temperature were assessed based on the obtained values from eqn (7) and (8), respectively, considering the concentrations of Cd(II) at the half saturation states of DA, ZD, and C/ZD ($C_{1/2}$) in addition to the values of translation partition (Z_v), $N_{m(Cd(II))}$, and $n_{(Cd(II))}$.[60]

$$\frac{E_{int}}{K_B T} = n N_m \left[\left(\frac{\left(\frac{C}{C_{1/2}}\right)^n \ln\left(\frac{C}{Z_v}\right)}{1 + \left(\frac{C}{C_{1/2}}\right)^n} \right) - \left(\frac{n \ln\left(\frac{C}{C_{1/2}}\right)\left(\frac{C}{C_{1/2}}\right)^n}{1 + \left(\frac{C}{C_{1/2}}\right)^n} \right) \right] \quad (7)$$

$$\frac{G}{K_B T} = n N_m \frac{\ln\left(\frac{C}{Z_v}\right)}{1 + \left(\frac{C_{1/2}}{C}\right)^n} \quad (8)$$

The negative signs of the obtained values of E_{int} for the conducting Cd(II) uptake processes by DA, ZD, and C/ZD, in addition to the remarkable declination in these values by increasing the tested temperature from 293 K to 303 K, validate the spontaneous and exothermic properties of these uptake processes (Fig. 8D–F). The same behaviors and properties were recorded for the determined values of enthalpy. The G values are negatively signed and display a reversible relation with the uptake temperature suggested declination in the feasibility properties of the uptake Cd(II) reactions by DA, ZD, and C/ZD in addition to their exothermic and spontaneous nature (Fig. 8G–I).

3.2.4. Recyclability. The recyclability investigation of DA, ZD, and C/ZD as Cd(II) adsorbents is critical to assessing the product for industrial use and practical applications. As regenerating stage, the used adsorbent particles were rinsed with HCL (10%) and sodium hydroxide (0.02 M) for a period of 60 minutes at 50 °C. The regenerating fractions were subsequently dried at 60 °C over 10 hours before being utilized in the re-adsorption of Cd(II) throughout five reusability runs. Following this, they had been washed several times using distilled water. The crucial elements were chosen at specific values, including volume (200 mL), duration (24 h), solid dose (0.2 g L^{-1}), temperature (20 °C), pH (7), and concentration (100 mg L^{-1}). Depending on the measured quantities of Cd(II) that were adsorbed, the synthetic structures exhibit significant stability and excellent recyclable properties (Fig. 9). For the recyclability value of DA during the adsorption of Cd(II), the measured adsorbed quantities are 78.4 mg g^{-1} (Cycle 1), 75.3 mg g^{-1} (Cycle 2), 67.3 mg g^{-1} (Cycle 3), 56.2 mg g^{-1} (Cycle 4), and 42.3 mg g^{-1} (Cycle 5) (Fig. 9). For ZD, the obtained adsorption capacities of Cd(II) during the recyclability cycles are 97.7 mg g^{-1} (Cycle 1), 96.3 mg g^{-1} (Cycle 2), 90.2 mg g^{-1} (Cycle 3), 81.3 mg g^{-1} (Cycle 4), and 74.2 mg g^{-1} (Cycle 5) (Fig. 9). Regarding the reusability of C/ZD, the determined uptake capacities of Cd(II) are 117.2 mg g^{-1} (Cycle 1), 116.3 mg g^{-1} (Cycle 2), 113.4 mg g^{-1} (Cycle 3), 108.6 mg g^{-1} (Cycle 4), and 102.2 mg g^{-1} (Cycle 5) (Fig. 9). The detected slight decrease in C/ ZD-recognized performance with repeated reusability cycles could be attributed to the continually developing chemical complexes between the Cd(II) ions and the chemical framework of the adsorbents, besides the expected slight leaking of the combined parts during the regeneration steps.

3.2.5. Effect of competitive ions. The impact of the various dissolved ions on the effectiveness of the C/ZD during the decontamination processes of Cd(II) was assessed either in the presence of some metal ions (Pb(II), Zn(II), Cu(II), and Co(II)) or chemical anions (PO_4^{-3}, NO_3^-, and SO_4^{-2}). The crucial variables were chosen at specific values, including: volume (200 mL), duration (24 h), solid dose (0.2 g L^{-1}), temperature (20 °C), pH (7), and concentration (100 mg L^{-1}, 50% Cd(II) + 50% competitive ion) (Fig. 10). The findings that were presented revealed that the assessed ions had a considerable impact on the Cd(II) selectivity. Cd(II) adsorption capacity (117.2 mg g^{-1}) by C/ZD decreased to 37.6 mg g^{-1}, 50.4 mg g^{-1}, 97.6 mg g^{-1}, and 103.3 mg g^{-1} in the presence of Pb(II), Zn(II), Cu(II), and Co(II) as competing ions, sequentially (Fig. 10). Such findings demonstrated the substantial impact of Pb(II) and Zn(II) ions during the retention of Cd(II). The findings revealed that other types of metal ions had a major negative impact on the uptake affinity of Cd(II) by C/ZD; nevertheless, they further demonstrated that the produced bio-composite seemed very effective at decontaminating several species of dangerous metal ions.

PO_4^{-3}, NO_3^-, and SO_4^{-2} had almost no effect on Cd(II) adsorption processes using C/ZD composite (Fig. 10). The phosphate anions had the most competitive impact, which was correlated with their propensities to form interior complexes with the hydroxyl groups within both cellulose and zeolitized diatomite. In comparison to PO_4^{-3}, the NO_3^- and SO_4^{-2} ions exhibit lower competitive characteristics because they have a larger propensity to form the outer-sphere complexes rather than the interior complexes, which have been identified for the adsorbed Cd(II). These findings display that the C/ZD composite has efficient adsorption characteristics for the practical removal
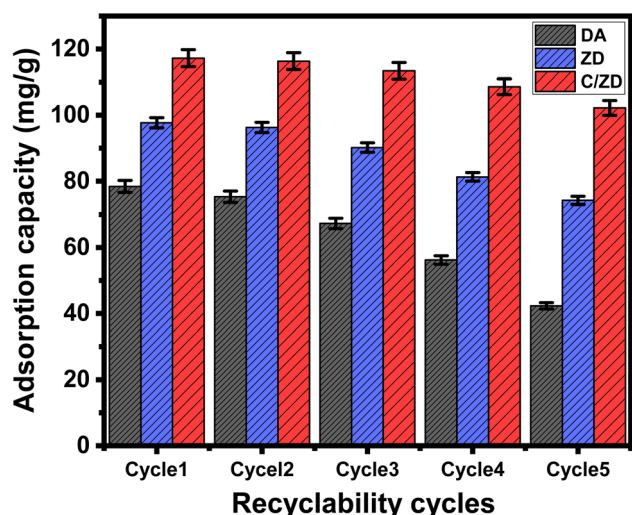

Fig. 9 The recyclability properties of DA, ZD, and C/ZD composite during the decontamination of Cd(II) ions.
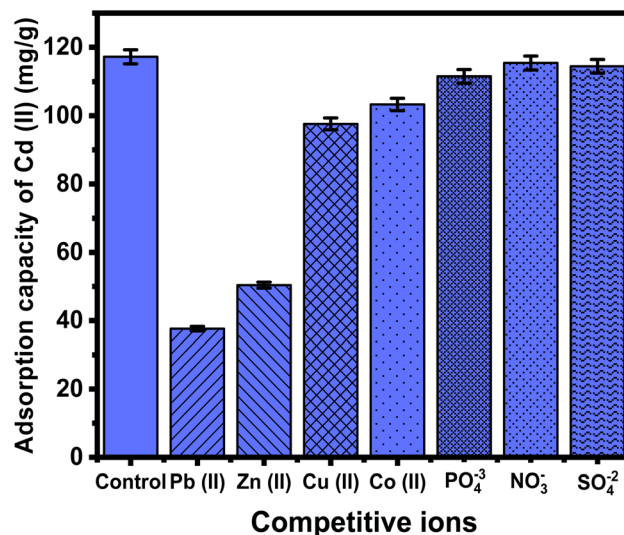

Fig. 10 The recyclability properties of DA, ZD, and C/ZD composite during the decontamination of Cd(II) ions.

Table 4 Comparison study for the adsorption capacities of the synthetic structure and other studies adsorbents

Adsorbent	Q_{max} (mg g^{-1})	References
Maghemite/MWCNTs	78.18	64
MCM-41/thioglycolic acid	91.3	65
Fe$_3$O$_4$-chitosan@bentonite	62.1	66
Magnetic MCM-48	114.08	67
Graphene oxide	23.9	68
Oxidized CNTs	92.59	69
Amino functional SBA-15	93.3	70
Canna indica based biochar	140.01	71
β-cyclodextrin/zeolite	93.06	72
MnO$_2$/MWCNTs	41.6	73
Attapulgite/CoFe$_2$O$_4$@SiO$_2$-chitosan/EDTA	127.79	74
Zeolite/zerovalent iron (Z-NZVI)	62.02	75
MCM-48	79.3	46
Ti-MCM-48	83.57	76
Chitosan/vermiculite	58.48	77
Composite chitosan biosorbent	108.7	78
Activated carbon	26.36	79
Magnetic chitosan-phenylthiourea resin	120	80
DA	127.8	This study
ZD	180.8	This study
C/ZD	229.4	This study

of Cd(II) from wastewater, regardless of the presence of different species of dissolved metal ions or other chemical anions, considering the tested concentration (100 mg L^{-1}).

3.2.6. Comparison study. The established capacities of DA and ZD as individual components have been compared with the Cd(II) adsorption characteristics of the C/ZD composite as well as other investigated adsorbents in the literature. While the measured Cd(II) adsorption capacity of C/ZD is 229.4 mg g^{-1} (Table 4), the observed capacities of diatomite (DA) and zeolitized diatomite (ZD) as separating components are 127.8 mg g^{-1} and 180.8 mg g^{-1}, respectively. These findings reveal that the zeolitization step and the integration of cellulose chains with zeolitized diatomite significantly increased the adsorption effectiveness of Cd(II). This may be connected to the impact of the cellulose integration on producing additional functional groups that are active uptake sites. Furthermore, the observed increase in surface area encourages contact and collision possibilities between Cd(II) and the active free sites of C/ZD grains. Additionally, the determined capacity of C/ZD is higher than the reported values for some of the previously studied adsorbents such as clay-based products (vermiculite, bentonite, attapulgite), CNTs based adsorbents (oxidized CNTs, maghemite/MWCNTs, and MnO$_2$/MWCNTs), graphene oxide, activated carbon, biochar, mesoporous silica based adsorbents (MCM-41/thioglycolic acid, magnetic MCM-48, SBA-15, Ti-MCM-48), zeolite based adsorbents (zeolite/zerovalent iron, β-cyclodextrin/zeolite, hydroxyapatite, and several studied chitosan-based adsorbents (Table 4)).

4 Conclusion

The siliceous frustules of diatomite were successfully turned into synthetic zeolite (ZD), which was then made to work better by adding cellulose fiber (C/ZD). The desorption properties were

assessed in a synergetic study bed on the steric and energetic parameters. The C/ZD composite exhibits a higher capacity (229.4 mg g^{-1}) than ZD (180.8 mg g^{-1}) and DA (127.8 mg g^{-1}), signifying the enhancing effect of the zeolitization and cellulose functionalization processes on the physicochemical properties of diatomite. The modification processes resulted in enhanced surface area and ion exchange capacity, in addition to the incorporation of additional active sites. This was supported by the recognized active site density as a steric parameter ($N_m = 98.46$ mg g^{-1} (C/ZD), 62.37 mg g^{-1} (ZD), and 37.2 mg g^{-1} (DA)) and the number of adsorbed Cd(II) per each active site ($n = 98.46$ mg g^{-1} (C/ZD), 62.37 mg g^{-1} (ZD), and 37.2 mg g^{-1} (DA)). The energetic findings, including both Gaussian energy (<8 kJ mol^{-1}) and retention energy (<8 kJ mol^{-1}), reflected no significant changes in the affecting physical adsorption mechanisms (van der Waals forces, dipole forces, ion exchange reaction) by the two modified products. These mechanisms display exothermic and spontaneous properties considering the investigated entropy, intern energy, and free enthalpy properties.

Conflicts of interest

There are no conflicts to declare.

Acknowledgements

References

1 M. Sajid, S. M. S. Jillani, N. Baig and K. Alhooshani, Layered double hydroxide-modified membranes for water treatment: Recent advances and prospects, *Chemosphere*, 2022, **287**, 132140.

2 X. Yang, J. Wang, A. M. El-Sherbeeny, A. A. AlHammadi, W.-H. Park and M. R. Abukhadra, Insight into the adsorption and oxidation activity of a ZnO/piezoelectric quartz core-shell for enhanced decontamination of ibuprofen: steric, energetic, and oxidation studies, *Chem. Eng. J.*, 2022, **431**, 134312.

3 M. Abdel Salam, M. Mokhtar, S. M. Albukhari, D. F. Baamer, L. Palmisano, M. Jaremko and M. R. Abukhadra, Synthesis and Characterization of Green ZnO@ polynaniline/ Bentonite Tripartite Structure (G. Zn@ PN/BE) as Adsorbent for As (V) Ions: Integration, Steric, and Energetic Properties, *Polymers*, 2022, **14**(12), 2329.

4 M. R. Abukhadra, M. H. Shemy, J. S. Khim, J. S. Ajarem, A. M. Rabie, A. A. Abdelrahman, A. A. Allam, H. M. Salem and M. S. Shaban, Insight into the Adsorption Properties of β-Cyclodextrin/Zeolite-A Structure for Effective Removal of Cd^{2+}, PO$_4^{3-}$, and Methyl Parathion; Kinetics and Advanced Equilibrium Studies, *J. Inorg. Organomet. Polym. Mater.*, 2022, 1–15.

5 R. Benisha, M. Amalanathan, M. Aravind, M. S. M. Mary, A. Ahmad and S. Tabassum, Catharanthus roseus leaf extract mediated Ag-MgO nanocatalyst for photocatalytic degradation of Congo red dye and their antibacterial activity, *J. Mol. Struct.*, 2022, **1262**, 133005.

6 S. M. Albukhari, M. A. Salam and M. R. Abukhadra, Effective retention of inorganic Selenium ions (Se (VI) and Se (IV)) using novel sodalite structures from muscovite; characterization and mechanism, *J. Taiwan Inst. Chem. Eng.*, 2021, **120**, 116–126.

7 I. R. Sayed, A. M. Farhan, A. A. AlHammadi, M. I. El-Sayed, I. M. Abd El-Gaied, A. M. El-Sherbeeny, W. Al Zoubi, Y. G. Ko and M. R. Abukhadra, Synthesis of novel nanoporous zinc phosphate/hydroxyapatite nano-rods (ZPh/HPANRs) core/shell for enhanced adsorption of Ni^{2+} and Co^{2+} ions: Characterization and application, *J. Mol. Liq.*, 2022, **360**, 119527.

8 F. Javaheri, Z. Kheshti, S. Ghasemi and A. Altaee, Enhancement of Cd^{2+} removal from aqueous solution by multifunctional mesoporous mesoporous silica: Equilibrium isotherms and kinetics study, *Sep. Purif. Technol.*, 2019, **224**, 199–208.

9 B. E. Igiri, S. I. Okoduwa, G. O. Idoko, E. P. Akabuogu, A. O. Adeyi and I. K. Ejiogu, Toxicity and bioremediation of heavy metals contaminated ecosystem from tannery wastewater: a review, *J. Toxicol.*, 2018, 2568038.

10 J. Xu, Z. Cao, Y. Zhang, Z. Yuan, Z. Lou, X. Xu and X. Wang, A review of functionalized carbon nanotubes and graphene for heavy metal adsorption from water: Preparation, application, and mechanism, *Chemosphere*, 2018, **195**, 351–364.

11 N. Nasser, M. I. El-Sayed, S. I. Othman, A. A. Allam, I. G. Al-Labadi, M. R. Abukhadra and S. Bellucci, Systematic Evaluation for the Impact of the Geological Conditions on the Adsorption Affinities of Calcite as an Adsorbent of Zn2+ Ions from Aqueous Solutions: Experimental and Theoretical Studies, *Minerals*, 2022, **12**(12), 1635.

12 R. Brandes, D. Belosinschi, F. Brouillette and B. Chabot, A new electrospun chitosan/phosphorylated nanocellulose biosorbent for the removal of cadmium ions from aqueous solutions, *J. Environ. Chem. Eng.*, 2019, **7**(6), 103477.

13 M. Shaban and M. R. Abukhadra, Geochemical evaluation and environmental application of Yemeni natural zeolite as sorbent for Cd^{2+} from solution: kinetic modeling, equilibrium studies, and statistical optimization, *Environ. Earth Sci.*, 2017, **76**, 1–16.

14 M. R. Abukhadra, M. Mostafa, M. N. B. Jumah, N. Al-Khalawi, R. S. Alruhaimi, Y. F. Salama and A. A. Allam, Insight into the Adsorption Properties of Chitosan/Zeolite-A Hybrid Structure for Effective Decontamination of Toxic Cd (II) and As (V) Ions from the Aqueous Environments, *J. Polym. Environ.*, 2022, **30**(1), 295–307.

15 P. B. Vilela, C. A. Matias, A. Dalalibera, V. A. Becegato and A. T. Paulino, Polyacrylic acid-based and chitosan-based hydrogels for adsorption of cadmium: equilibrium isotherm, kinetic and thermodynamic studies, *J. Environ. Chem. Eng.*, 2019, **7**(5), 103327.

16 V. Souza-Arroyo, J. J. Fabián, L. Bucio-Ortiz, R. U. Miranda-Labra, L. E. Gomez-Quiroz and M. C. Gutiérrez-Ruiz, The mechanism of the cadmium-induced toxicity and cellular response in the liver, *Toxicology*, 2022, 153339.

17 T. El Rasafi, A. Oukarroum, A. Haddioui, H. Song, E. E. Kwon, N. Bolan, F. M. Tack, A. Sebastian, M. N. V. Prasad and J. Rinklebe, Cadmium stress in plants: a critical review of the effects, mechanisms, and tolerance strategies, *Crit. Rev. Environ. Sci. Technol.*, 2022, **52**(5), 675–726.

18 E. A. Ofudje, A. E. Adedapo, O. B. Oladeji, E. F. Sodiya, F. H. Ibadin and D. Zhang, Nano-rod hydroxyapatite for the uptake of nickel ions: Effect of sintering behaviour on adsorption parameters, *J. Environ. Chem. Eng.*, 2021, **9**(5), 105931.

19 A. M. El-Sherbeeny, S. M. Ibrahim, A. A. AlHammadi, A. T. A. Soliman, J. J. Shim and M. R. Abukhadra, Effective retention of radioactive Cs^+ and Ba^{2+} ions using β-cyclodextrin functionalized diatomite (β-CD/D) as environmental adsorbent; characterization, application, and safety, *Surf. Interfaces*, 2021, **26**, 101434.

20 A. Kadeche, A. Ramdani, M. Adjdir, A. Guendouzi, S. Taleb, M. Kaid and A. Deratani, Preparation, characterization and application of Fe-pillared bentonite to the removal of Coomassie blue dye from aqueous solutions, *Res. Chem. Intermed.*, 2020, **46**(11), 4985–5008.

21 Y. Chen, Z. Nie, J. Gao, J. Wang and M. Cai, A novel adsorbent of bentonite modified chitosan-microcrystalline cellulose aerogel prepared by bidirectional regeneration strategy for Pb (II) removal, *J. Environ. Chem. Eng.*, 2021, **9**(4), 105755.

22 C. A. Raju, J. Anitha, R. M. Kalyani, K. Satyanandam and P. Jagadeesh, Sorption of cobalt using marine macro seaweed graciliariacorticatared algae powder, *Mater. Today: Proc.*, 2021, **44**, 1816–1827.

23 A. S. Mohamed, M. R. Abukkhadra, E. A. Abdallah, A. M. El-Sherbeeny and R. K. Mahmoud, The photocatalytic performance of silica fume based Co3O4/MCM-41 green nanocomposite for instantaneous degradation of Omethoate pesticide under visible light, *J. Photochem. Photobiol., A*, 2020, **392**, 112434.

24 S. M. Ibrahim, M. N. Bin Jumah, S. I. Othman, R. S. Alruhaimi, N. Al-Khalawi, Y. F. Salama, A. A. Allam and M. R. Abukhadra, Synthesis of Chitosan/Diatomite Composite as an Advanced Delivery System for Ibuprofen Drug; Equilibrium Studies and the Release Profile, *ACS Omega*, 2021, **6**(20), 13406–13416.

25 L. Fan, W. Kong, C. Gao and P. Zhu, Synthesis of highly porous iron-doped carbonated hydroxyapatite spheres for efficient adsorption of carmine dyes, *Materialia*, 2021, **20**, 101205.

26 M. N. B. Jumah, M. H. Eid, A. A. AL-Huqail, M. A. Mohammad, N. S. Bin-Murdhi, G. M. Abu-Taweel, N. Altoom, A. A. Allam and M. R. AbuKhadra, Enhanced remediation of As (V) and Hg (II) ions from aqueous environments using β-cyclodextrin/MCM-48 composite:

batch and column studies, *J. Water Process. Eng.*, 2021, **42**, 102118.

27 C. Tramontano, B. Miranda, G. Chianese, L. De Stefano, C. Forestiere, M. Pirozzi and I. Rea, Design of gelatin-capped plasmonic-diatomite nanoparticles with enhanced galunisertib loading capacity for drug delivery applications, *Int. J. Mol. Sci.*, 2021, **22**(19), 10755.

28 F. Zobi, Diatom biosilica in targeted drug delivery and biosensing applications: recent studies, *Micro*, 2022, **2**(2), 342–360.

29 G. Liu, M. R. Abukhadra, A. M. El-Sherbeeny, A. M. Mostafa and M. A. Elmeligy, Insight into the photocatalytic properties of diatomite@ Ni/NiO composite for effective photo-degradation of malachite green dye and photo-reduction of Cr (VI) under visible light, *J. Environ. Manage.*, 2020, **254**, 109799.

30 F. Shajarat, K. Ghanemi, M. Alimoradi and M. Ramezani, Nanostructured composite of polydopamine/diatomite–based biosilica to enhance the extraction of phthalate esters from aqueous samples, *Microchem. J.*, 2022, **174**, 107060.

31 F. Baba, F. Benaliouche, R. Meknaci and Y. Boucheffa, Water adsorption and antibacterial activity studies for characterization of Ca-LTA zeolite/diatomite adsorbents, *Colloid Interface Sci. Commun.*, 2020, **35**, 100233.

32 J. M. Moreno-Maroto, J. Alonso-Azcárate, C. Martínez-García, M. Romero, A. López-Delgado and T. Cotes-Palomino, Zeolitization of Diatomite Residues by a Simple Method, *Appl. Sci.*, 2022, **12**(21), 10977.

33 L. Sun, J. Wu, J. Wang, G. Yu, J. Liu, Y. Du, Y. Li and H. Li, Controlled synthesis of Zeolite adsorbent from low-grade diatomite: a case study of self-assembled sodalite microspheres, *J. Environ. Sci.*, 2020, **91**, 92–104.

34 M.-T. Ashraf, A. A. AlHammadi, A. M. El-Sherbeeny, S. Alhammadi, W. Al Zoubi, Y. G. Ko and M. R. Abukhadra, Synthesis of cellulose fibers/Zeolite-A nanocomposite as an environmental adsorbent for organic and inorganic selenium ions; characterization and advanced equilibrium studies, *J. Mol. Liq.*, 2022, **360**, 119573.

35 N. Altoom, M. T. Ashraf, S. M. Ibrahim, S. I. Othman, A. A. Allam, H. A. Alqhtani and M. R. Abukhadra, Insight into the loading, release, and anticancer properties of cellulose/zeolite-A as an enhanced delivery structure for oxaliplatin chemotherapy; characterization and mechanism, *J. Sol-Gel Sci. Technol.*, 2022, **103**(3), 752–765.

36 B. F. Dizaji, M. H. Azerbaijan, N. Sheisi, P. Goleij, T. Mirmajidi, F. Chogan, M. Irani and F. Sharafian, Synthesis of PLGA/chitosan/zeolites and PLGA/chitosan/metal organic frameworks nanofibers for targeted delivery of paclitaxel toward prostate cancer cells death, *Int. J. Biol. Macromol.*, 2020, **164**, 1461–1474.

37 M. Servatan, P. Zarrintaj, G. Mahmodi, S. J. Kim, M. R. Ganjali, M. R. Saeb and M. Mozafari, Zeolites in drug delivery: progress, challenges and opportunities, *Drug Discovery Today*, 2020, **25**, 642–656.

38 M. R. Abukhadra, F. A. El Kashief, S. I. Othman, H. A. Alqhtani and A. A. Allam, Synthesis and characterization of Fe⁰@ chitosan/cellulose biocompatible composites from natural resources as advanced carriers for ibuprofen drug: reaction kinetics and equilibrium, *New J. Chem.*, 2022, **46**(26), 12797–12807.

39 H. Abdul Khalil, A. Adnan, E. B. Yahya, N. Olaiya, S. Safrida, M. Hossain, V. Balakrishnan, D. A. Gopakumar, C. Abdullah and A. Oyekanmi, A review on plant cellulose nanofibre-based aerogels for biomedical applications, *Polymers*, 2020, **12**(8), 1759.

40 L. Tian, M. R. Abukhadra, A. S. Mohamed, A. Nadeem, S. F. Ahmad and K. E. Ibrahim, Insight into the loading and release properties of an exfoliated kaolinite/cellulose fiber (EXK/CF) composite as a carrier for oxaliplatin drug: cytotoxicity and release kinetics, *ACS Omega*, 2020, **5**(30), 19165–19173.

41 J. N. Putro, S. P. Santoso, S. Ismadji and Y. H. Ju, Investigation of heavy metal adsorption in binary system by nanocrystalline cellulose–bentonite nanocomposite: improvement on extended Langmuir isotherm model, *Microporous Mesoporous Mater.*, 2017, **246**, 166–177.

42 M. Pooresmaeil, S. Javanbakht, S. B. Nia and H. Namazi, Carboxymethyl cellulose/mesoporous magnetic graphene oxide as a safe and sustained ibuprofen delivery bio-system: synthesis, characterization, and study of drug release kinetic, *Colloids Surf., A*, 2020, **594**, 124662.

43 Y. Chen, L. Zhang, C. Mei, Y. Li, G. Duan, S. Agarwal, A. Greiner, C. Ma and S. Jiang, Wood-inspired anisotropic cellulose nanofibril composite sponges for multifunctional applications, *ACS Appl. Mater. Interfaces*, 2020, **12**(31), 35513–35522.

44 M. Mostafa, M. A. El-Meligy, M. Sharaf, A. T. Soliman and M. R. AbuKhadra, Insight into chitosan/zeolite-A nanocomposite as an advanced carrier for levofloxacin and its anti-inflammatory properties; loading, release, and anti-inflammatory studies, *Int. J. Biol. Macromol.*, 2021, **179**, 206–216.

45 E. L. Vivas and K. Cho, Efficient adsorptive removal of cobalt (II) ions from water by dicalcium phosphate dihydrate, *J. Environ. Manage.*, 2021, **283**, 111990.

46 M. Jiang, L. Chen and N. Niu, Enhanced adsorption for malachite green by functionalized lignin magnetic composites: optimization, performance and adsorption mechanism, *J. Mol. Struct.*, 2022, **1260**, 132842.

47 M. R. Abukhadra, B. M. Bakry, A. Adlii, S. M. Yakout and M. E. El-Zaidy, Facile conversion of kaolinite into clay nanotubes (KNTs) of enhanced adsorption properties for toxic heavy metals (Zn2+, Cd2+, Pb2+, and Cr6+) from water, *J. Hazard. Mater.*, 2019, **374**, 296–308.

48 E. El Qada, Kinetic Behavior of the Adsorption of Malachite Green Using Jordanian Diatomite as Adsorbent, *Jordanian J. Eng. Chem. Ind. Res. Pap.*, 2020, **3**, 1–10.

49 M. A. Salam, M. R. Abukhadra and M. Mostafa, Effective decontamination of As (V), Hg (II), and U (VI) toxic ions from water using novel muscovite/zeolite aluminosilicate composite: adsorption behavior and mechanism, *Environ. Sci. Pollut. Res.*, 2020, **27**(12), 13247–13260.

50 X. Lin, Y. Xie, H. Lu, Y. Xin, R. Altaf, S. Zhu and D. Liu, Facile preparation of dual La-Zr modified magnetite adsorbents for efficient and selective phosphorus recovery, *Chem. Eng. J.*, 2021, **413**, 127530.

51 A. Sherlala, A. Raman, M. M. Bello and A. Buthiyappan, Adsorption of arsenic using chitosan magnetic graphene oxide nanocomposite, *J. Environ. Manage.*, 2019, **246**, 547–556.

52 Y. Huang, X. Zeng, L. Guo, J. Lan, L. Zhang and D. Cao, Heavy metal ion removal of wastewater by zeolite-imidazolate frameworks, *Sep. Purif. Technol.*, 2018, **194**, 462–469.

53 E. E. Jasper, V. O. Ajibola and J. C. Onwuka, Nonlinear regression analysis of the sorption of crystal violet and methylene blue from aqueous solutions onto an agro-waste derived activated carbon, *Appl. Water Sci.*, 2020, **10**(6), 1–11.

54 C. Giles, T. MacEwan, S. Nakhwa and D. Smith, 786. Studies in adsorption. Part XI. A system of classification of solution adsorption isotherms, and its use in diagnosis of adsorption mechanisms and in measurement of specific surface areas of solids, *J. Chem. Soc.*, 1960, 3973–3993.

55 M. R. Abukhadra, F. M. Dardir, M. Shaban, E. A. Ahmed and M. F. Soliman, Superior removal of Co^{2+}, Cu^{2+} and Zn^{2+} contaminants from water utilizing spongy Ni/Fe carbonate–fluorapatite; preparation, application and mechanism, *Ecotoxicol. Environ. Saf.*, 2018, **157**, 358–368.

56 M. Shaban, M. R. Abukhadra, M. G. Shahien and A. A. P. Khan, Upgraded modified forms of bituminous coal for the removal of safranin-T dye from aqueous solution, *Environ. Sci. Pollut. Res.*, 2017, **24**(22), 18135–18151.

57 F. Dawodu, G. Akpomie and M. Abuh, Equilibrium Isotherm Studies on the Batch Sorption of Copper (II) ions from Aqueous Solution unto Nsu Clay, *Int. J. Sci. Eng. Res.*, 2012, **3**(12), 1–7.

58 M. Mobarak, R. A. Ali and M. K. Seliem, Chitosan/activated coal composite as an effective adsorbent for Mn (VII): modeling and interpretation of physicochemical parameters, *Int. J. Biol. Macromol.*, 2021, **186**, 750–758.

59 F. Dhaouadi, L. Sellaoui, H. E. Reynel-Ávila, V. Landín-Sandoval, D. I. Mendoza-Castillo, J. E. Jaime-Leal, E. C. Lima, A. Bonilla-Petriciolet and A. B. Lamine, Adsorption mechanism of Zn2+, Ni2+, Cd2+, and Cu2+ ions by carbon-based adsorbents: interpretation of the adsorption isotherms via physical modelling, *Environ. Sci. Pollut. Res.*, 2021, **28**(24), 30943–30954.

60 F. Dhaouadi, L. Sellaoui, M. Badawi, H. E. Reynel-Ávila, D. I. Mendoza-Castillo, J. E. Jaime-Leal, A. Bonilla-Petriciolet and A. B. Lamine, Statistical physics interpretation of the adsorption mechanism of Pb^{2+}, Cd^{2+} and Ni^{2+} on chicken feathers, *J. Mol. Liq.*, 2020, **319**, 114168.

61 L. Sellaoui, J. Ali, M. Badawi, A. Bonilla-Petriciolet and Z. Chen, Understanding the adsorption mechanism of Ag^+ and Hg^{2+} on functionalized layered double hydroxide via statistical physics modeling, *Appl. Clay Sci.*, 2020, **198**, 105828.

62 R. A. Ali, M. Mobarak, A. M. Badawy, E. C. Lima, M. K. Seliem and H. Ramadan, New insights into the surface oxidation role in enhancing Congo red dye uptake by Egyptian ilmenite ore: Experiments and physicochemical interpretations, *Surf. Interfaces*, 2021, **26**, 101316.

63 L. Sellaoui, H. Guedidi, L. Reinert, S. Knani, L. Duclaux and A. B. Lamine, Experimental and theoretical studies of adsorption of ibuprofen on raw and two chemically modified activated carbons: new physicochemical interpretations, *RSC Adv.*, 2016, **6**(15), 12363–12373.

64 M. P. Gatabi, H. M. Moghaddam and M. Ghorbani, Efficient removal of cadmium using magnetic multiwalled carbon nanotube nanoadsorbents: equilibrium, kinetic, and thermodynamic study, *J. Nanopart. Res.*, 2016, **18**, 189.

65 I. M. M. Kenawy, Y. A. El-Reash, M. M. Hassanien, N. R. Alnagar and W. I. Mortada, Use of microwave irradiation for modification of mesoporous silica nanoparticles by thioglycolic acid for removal of cadmium and mercury, *Microporous Mesoporous Mater.*, 2018, **258**, 217–227.

66 G. Feng, J. Ma, X. Zhang, Q. Zhang, Y. Xiao, Q. Ma and S. Wang, Magnetic natural composite Fe3O4-chitosan@bentonite for removal of heavy metals from acid mine drainage, *J. Colloid Interface Sci.*, 2019, **538**, 132–141.

67 M. Anbia, K. Kargosha and S. Khoshbooei, Heavy metal ions removal from aqueous media by modified magnetic mesoporous silica MCM-48, *Chem. Eng. Res. Des.*, 2015, **93**, 779–788.

68 Y. Bian, Z. Y. Bian, J. X. Zhang, A. Z. Ding, S. L. Liu and H. Wang, Effect of the oxygen-containing functional group of graphene oxide on the aqueous cadmium ions removal, *Appl. Surf. Sci.*, 2015, **329**, 269–275.

69 M. A. Tofighy and T. Mohammadi, Adsorption of divalent heavy metal ions from water using carbon nanotube sheets, *J. Hazard. Mater.*, 2011, **185**, 140–147.

70 J. Aguado, J. M. Arsuaga, A. Arencibia, M. Lindo and V. Gascón, Aqueous heavy metals removal by adsorption on amine-functionalized mesoporous silica, *J. Hazard. Mater.*, 2009, **163**(1), 213–221.

71 X. Cui, S. Fang, Y. Yao, T. Li, Q. Ni, X. Yang and Z. He, Potential mechanisms of cadmium removal from aqueous solution by Canna indica derived biochar, *Sci. Total Environ.*, 2016, **562**, 517–525.

72 S. Zheng, S. Xia, S. Han, F. Yao, H. Zhao and M. Huang, β-Cyclodextrin-loaded minerals as novel sorbents for enhanced adsorption of Cd^{2+} and Pb^{2+} from aqueous solutions, *Sci. Total Environ.*, 2019, **693**, 133676.

73 C. Luo, R. Wei, D. Guo, S. Zhang and S. Yan, Adsorption behavior of MnO_2 functionalized multi-walled carbon nanotubes for the removal of cadmium from aqueous solutions, *Chem. Eng. J.*, 2013, **225**, 406–415.

74 Y. Wang, R. Zhou, C. Wang, G. Zhou, C. Hua, Y. Cao and Z. Song, Novel environmental-friendly nano-composite magnetic attapulgite functionalized by chitosan and EDTA for cadmium (II) removal, *J. Alloys Compd.*, 2020, **817**, 153286.

75 Z. Li, L. Wang, J. Meng, X. Liu, J. Xu, F. Wang and P. Brookes, Zeolite-supported nanoscale zero-valent iron: New findings on simultaneous adsorption of Cd (II), Pb (II), and As (III)

in aqueous solution and soil, *J. Hazard. Mater.*, 2018, **344**, 1–11.

76 J. Chen, K. Fang, L. Wu, Z. Qian and J. Chen, Removal of Cd (II) from aqueous by adsorption onto mesoporous Ti-MCM-48, *Procedia Environ. Sci.*, 2011, **10**, 2491–2497.

77 L. Chen, P. Wu, M. Chen, X. Lai, Z. Ahmed, N. Zhu, Z. Dang, Y. Bi and T. Liu, Preparation and characterization of the eco-friendly chitosan/vermiculite biocomposite with excellent removal capacity for cadmium and lead, *Appl. Clay Sci.*, 2018, **159**, 74–82.

78 S. Madala, S. K. Nadavala, S. Vudagandla, V. M. Boddu and K. Abburi, Equilibrium, kinetics and thermodynamics of cadmium (II) biosorption on to composite chitosan biosorbent, *Arabian J. Chem.*, 2017, **10**, 1883–1893.

79 D. Obregón-Valencia and M. del Rosario Sun-Kou, Comparative cadmium adsorption study on activated carbon prepared from aguaje (Mauritiaflexuosa) and olive fruit stones (Olea europaea L.), *J. Environ. Chem. Eng.*, 2014, **2**(4), 280–2288.

80 M. Monier and D. A. Abdel-Latif, Preparation of cross-linked magnetic chitosan-phenylthiourea resin for adsorption of Hg(II), Cd(II) and Zn(II) ions from aqueous solutions, *J. Hazard. Mater.*, 2012, **209–210**, 240–249.